6. Stockmeyer B, Beyer T, Neuhuber W, Repp R, Kalden JR, Valerius T and Herrmann M: Polymorphonuclear granulocytes induce antibody-dependent apoptosis in human breast cancer cells. J Immunol 171: 5124-5129, 2003.
7. Challacombe JM, Suhrbier A, Parsons PG, Jones B, Hampson P, Kavanagh D, Rainger GE, Morris M, Lord JM, Le TT, Hoang-Le D and Ogbourne SM: Neutrophils are a key component of the antitumor efficacy of topical chemotherapy with ingenol-3-angelate. J Immunol 177: 8123-8132, 2006.
8. Koga Y, Matsuzaki A, Suminoe A, Hattori H and Hara T: Neutrophil-derived TNF-related apoptosis-inducing ligand (TRAIL): a novel mechanism of antitumor effect by neutrophils. Cancer Res 64: 1037-1043, 2004.
9. Kemp TJ, Ludwig AT, Earel JK, Moore JM, Vanoosten RL, Moses B, Leidal K, Nauseef WM and Griffith TS: Neutrophil stimulation with Mycobacterium bovis bacillus Calmette-Guérin (BCG) results in the release of functional soluble TRAIL/Apo-2L. Blood 106: 3474-3482, 2005.
10. de Vries EG, Gietema JA and de Jong S: Tumor necrosis factor-related apoptosis-inducing ligand pathway and its therapeutic implications. Clin Cancer Res 12: 2390-2393, 2006.
11. Voortman J, Resende TP, Abou EI Hassan MA, Giaccone G and Kruyt FA: TRAIL therapy in non-small cell lung cancer cells: sensitization to death receptor-mediated apoptosis by proteasome inhibitor bortezomib. Mol Cancer Ther 6: 2103-2112, 2007.
12. Hoshi H, Sawada T, Uchida M, Saito H, Iijima H, Toda-Agetsuma M, Wada T, Yamazoe S, Tanaka H, Kimura K, Kakehashi A, Wei M, Hirakawa K and Wanibuchi H: Tumor-associated MUC5AC stimulates *in vivo* tumorigenicity of human pancreatic cancer. Int J Oncol 38: 619-627, 2011.
13. Hernandez-Ilizaliturri FJ, Jupudy V, Ostberg J, Oflazoglu E, Huberman A, Repasky E and Czuczman MS: Neutrophils contribute to the biological antitumor activity of rituximab in a non-Hodgkin's lymphoma severe combined immunodeficiency mouse model. Clin Cancer Res 9: 5866-5873, 2003.
14. Singh PK and Hollingsworth MA: Cell surface-associated mucins in signal transduction. Trends Cell Biol 16: 467-476, 2006.
15. Lane D, Côté M, Grondin R, Couture MC and Piché A: Acquired resistance to TRAIL-induced apoptosis in human ovarian cancer cells is conferred by increased turnover of mature caspase-3. Mol Cancer Ther 5: 509-521, 2006.
16. Lane D, Robert V, Grondin R, Rancourt C and Piché A: Malignant ascites protect against TRAIL-induced apoptosis by activating the PI3K/Akt pathway in human ovarian carcinoma cells. Int J Cancer 121: 1227-1237, 2007.
17. Di Carlo E, Forni G, Lollini P, Colombo MP, Modesti A and Musiani P: The intriguing role of polymorphonuclear neutrophils in antitumor reactions. Blood 97: 339-345, 2001.
18. Alvarez MJ, Prada F, Salvatierra E, Bravo AI, Lutzky VP, Carbone C, Pitossi FJ, Chuluyan HE and Podhajcer OL: Secreted protein acidic and rich in cysteine produced by human melanoma cells modulates polymorphonuclear leukocyte recruitment and antitumor cytotoxic capacity. Cancer Res 65: 5123-5132, 2005.
19. Chen YL, Chen SH, Wang JY and Yang BC: Fas ligand on tumor cells mediates inactivation of neutrophils. J Immunol 171: 1183-1191, 2003.
20. Sanford MA, Yan Y, Canfield SE, Hassan W, Selleck WA, Atkinson G, Chen SH and Hall SJ: Independent contributions of GR-1+ leukocytes and Fas/FasL interactions to induce apoptosis following interleukin-12 gene therapy in a metastatic model of prostate cancer. Hum Gene Ther 12: 1485-1498, 2001.
21. Niitsu N, Khori M, Hayama M, Kajiwara K, Higashihara M and Tamaru J: Phase I/II study of the rituximab-EPOCT regimen in combination with granulocyte colony-stimulating factor in patients with relapsed or refractory follicular lymphoma including evaluation of its cardiotoxicity using B-type natriuretic peptide and troponin T levels. Clin Cancer Res 11: 697-702, 2005.
22. Otten MA, Rudolph E, Dechant M, Tuk CW, Reijmers RM, Beelen RH, van de Winkel JG and van Egmond M: Immature neutrophils mediate tumor cell killing via IgA but not IgG Fc receptors. J Immunol 174: 5472-5480, 2005.
23. Wiley SR, Schooley K, Smolak PJ, Din WS, Huang CP, Nicholl JK, Sutherland GR, Smith TD, Rauch C, Smith CA and Goodwin RG: Identification and characterization of a new member of the TNF family that induces apoptosis. Immunity 3: 673-682, 1995.
24. Schimmer AD: Inhibition of apoptosis proteins: translating basic knowledge into clinical practice. Cancer Res 64: 7183-7190, 2004.
25. Wei Y, Fan T and Yu M: Inhibitor of apoptosis proteins and apoptosis. Acta Biochim Biophys Sin (Shanghai) 40: 278-288, 2009.
26. Komatsu M, Jepson S, Arango ME, Carraway CAC and Carraway KL: Muc4/sialomucin complex, an intramembrane modulator of ErbB2/HER2/Neu, potentiates primary tumor growth and suppresses apoptosis in a xenotransplanted tumor. Oncogene 20: 461-470, 2001.
27. Workman HC, Sweeney C, Carraway KL III: The membrane mucin Muc4 inhibits apoptosis induced by multiple insults via ErbB2-dependent and ErbB2-independent mechanisms. Cancer Res 69: 2845-2852, 2009.
28. Baratelli F, Krysan K, Heuzé-Vourc'h N, Zhu L, Escuadro B, Sharma S, Reckamp K, Dohadwala M and Dubinett SM: PGE2 confers survivin-dependent apoptosis resistance in human monocyte-derived dendritic cells. J Leukoc Biol 78: 555-564, 2005.
29. Leone V, di Palma A, Ricchi P, Acquaviva F, Giannouli M, Di Prisco AM, Iuliano F and Acquaviva AM: PGE2 inhibits apoptosis in human adenocarcinoma Caco-2 cell line through Ras-PI3K association and cAMP-dependent kinase A activation. Am J Physiol Gastrointest Liver Physiol 293: G673-G681, 2007.

SCIENTIFIC REPORTS

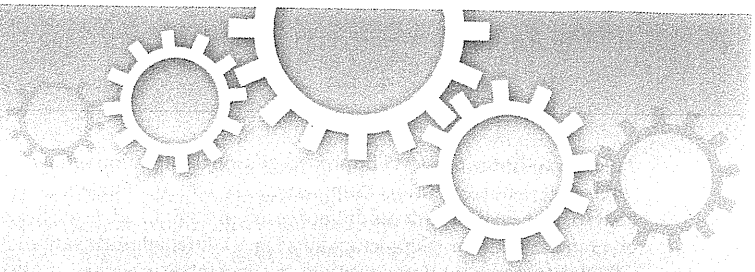

OPEN

SUBJECT AREAS:
DRUG DISCOVERY AND DEVELOPMENT
NEURODEVELOPMENTAL DISORDERS
DEVELOPMENTAL DISORDERS
MOLECULAR NEUROSCIENCE

Received
11 October 2012

Accepted
15 January 2013

Published
6 February 2013

Correspondence and requests for materials should be addressed to S.H. (shinjih@med.osaka-cu.ac.jp)

* These authors contributed equally to this work.

# Post-natal treatment by a blood-brain-barrier permeable calpain inhibitor, SNJ1945 rescued defective function in lissencephaly

Shiori Toba[1]*, Yasuhisa Tamura[2]*, Kanako Kumamoto[1]*, Masami Yamada[1], Keizo Takao[3,4], Satoko Hattori[3,5], Tsuyoshi Miyakawa[3,4,5], Yosky Kataoka[2], Mitsuyoshi Azuma[6], Kiyoshi Hayasaka[7], Masano Amamoto[8], Keiko Tominaga[9], Anthony Wynshaw-Boris[10], Hideki Wanibuchi[11], Yuichiro Oka[12,13,14], Makoto Sato[12,13,14], Mitsuhiro Kato[7] & Shinji Hirotsune[1]

[1]Department of Genetic Disease Research, Osaka City University Graduate School of Medicine, Asahi-machi 1-4-3 Abeno, Osaka 545-8586, Japan, [2]Cellular Function Imaging Laboratory, RIKEN Center for Molecular Imaging Science, Minatojima minamimachi, Chuo-ku, Kobe, Hyogo, Japan, [3]Japan Science and Technology Agency, CREST, 4-1-8 Honcho, Kawaguchi, Saitama 332-0012, Japan, [4]Section of Behavior Patterns, Center for Genetic Analysis of Behavior National Institute for Physiological Sciences, 38 Nishigonaka Myodaiji, Okazaki, Aichi, 444-8585, Japan, [5]Division of Systems Medical Science, Institute for Comprehensive Medical Science, Fujita Health University, Toyoake, Aichi 470-1192, Japan, [6]Senju Laboratory of Ocular Sciences, Senju Pharmaceutical Co., Ltd., 1-5-4, Murotani, Nishi-ku, Kobe, Hyogo 651-2241, Japan, [7]Department of Pediatrics, Yamagata University Faculty of Medicine, Iida-nishi 2-2-2, Yamagata 990-9585, Japan, [8]Pediatric Emergency Center, Kitakyuusyu City Yahata Hospital. Nishimotomachi 4-18-1, Yahatahigasi Kitakyuusyu City, Japan, [9]Department of Internal Medicine, Tokyo Metropolitan Fuchu Medical Center for the Disabled. Musashidai, Fuchu-shi, Tokyo, Japan, [10]Department of Pediatrics and Institute for Human Genetics, University of California, San Francisco, School of Medicine, San Francisco, CA 94143-0794, [11]Department of Pathology, Osaka City University Graduate School of Medicine, Asahi-machi 1-4-3 Abeno, Osaka 545-8586, Japan, [12]Division of Cell Biology and Neuroscience, Department of Morphological and Physiological Sciences, Faculty of Medical Sciences, University of Fukui, [13]Research Center for Child Mental Development, University of Fukui, [14]Research and Education Program for Life Science, University of Fukui.

**Toward a therapeutic intervention of lissencephaly, we applied a novel calpain inhibitor, SNJ1945. Peri-natal or post-natal treatment with SNJ1945 rescued defective neuronal migration in *Lis1*$^{+/-}$ mice, impaired behavioral performance and improvement of $^{18}$F-FDG uptake. Furthermore, SNJ1945 improved the neural circuit formation and retrograde transport of NFG in *Lis1*$^{+/-}$ mice. Thus, SNJ1945 is a potential drug for the treatment of human lissencephaly patients.**

LIS1 encodes a protein carrying seven WD repeats[1,2] that was first identified as a non-catalytic subunit of platelet activating factor-acetylhydrolase (Pafah1b1)[3]. Numerous studies to address the molecular function of LIS1 led to the conclusion that LIS1 is essential for the proper regulation of cytoplasmic dynein[4–6]. We previously reported that calpain inhibition rescued defective phenotypes that are observed in *Lis1*$^{+/-}$ mice[7], suggesting that calpain inhibitors are a potential therapy for the treatment of lissencephaly. Here, we applied a novel blood-brain barrier (BBB) permeable calpain inhibitor, SNJ1945 for the treatment of lissencephaly[8–10].

## Results

**SNJ1945 rescued defective distribution of cytoplasmic dynein and membranous components in the cell and defective migration in *Lis1*$^{+/-}$ neurons.** *In vitro* administration of SNJ1945 protected LIS1 from proteolysis, resulting in the augmentation of LIS1 levels in *Lis1*$^{+/-}$ mouse embryonic fibroblast (MEF) cells and leading to rescue of the aberrant distribution of cytoplasmic dynein and intracellular components including mitochondria and β-COP positive vesicles (Supplementary Fig. 1a–e). SNJ1945 also rescued defective distribution of cytoplasmic dynein and membranous components in human fibroblasts from an isolated lissencephaly sequence (ILS) patient, suggesting that SNJ1945 will be similarly effective in the human (Supplementary Fig.

2a–e). In addition, SNJ1945 improved neuronal migration of *Lis1*$^{+/-}$ cerebellar granular neurons (Supplementary Fig. 3). Notably, administration of even large doses did not result in obvious adverse effects on granular neurons (Supplementary Fig. 4). Oral administration of SNJ1945 to pregnant dams resulted in substantial increases of LIS1 levels in the brain of fetuses, as did oral administration directly to peri-natal offspring or adults (Fig. 1). Importantly, LIS1 levels increased in the brain three weeks after birth (Fig. 1c, f), indicating that indeed SNJ1945 passed through the BBB and inhibited proteolytic degradation of LIS1. Quantitative determination of drug concentrations in tissue homogenates via liquid chromatography-tandem mass spectrometry (LC-MS/MS) is commonly conducted using the standards. We measured the concentration of SNJ1945 in the brain using LC-MS/MS (Supplementary table 1). LC-MS/MS analysis indicated the brain distribution of SNJ 1945.

To demonstrate whether there was therapeutic benefit *in vivo*, we designed four different administration approaches (Fig. 2a): (1) intra-peritoneal injection starting at E9.5 (100 μg/g) followed by oral

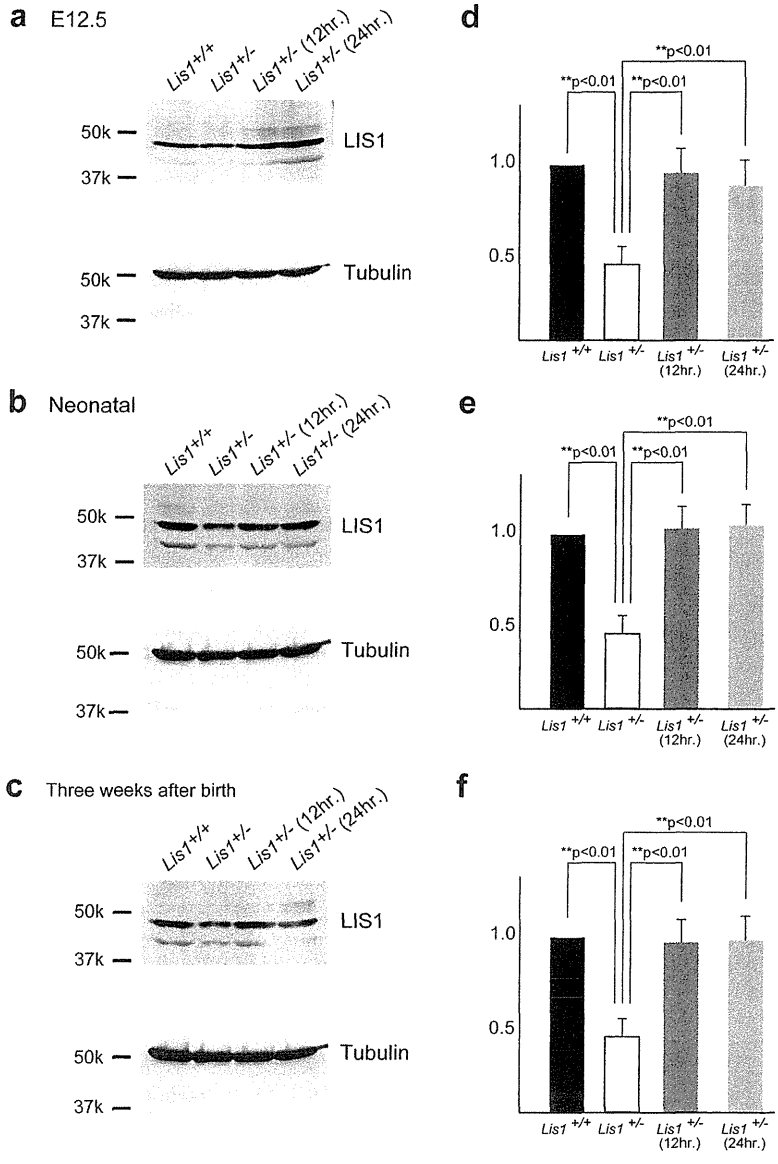


**Figure 1 | Rescue of defective corticogenesis in *Lis1*$^{+/-}$ mice by SNJ1945.** (a, b, c) Western blotting analysis of the brain after treatment of SNJ1945. Western blotting was performed on brain lysates after oral administration of SNJ1945. Time after oral administration is indicated at the top. Antibodies used for Western blots are indicated at the right of the Western blotting panels. Size maker and each molecular weight were shown at the left. Protein levels were normalized to tubulin beta-3 (Tubulin) as a control and are indicated at a graph (d, e, f). Statistical examination was performed by unpaired Student's *t*-test at 12 and 24 hrs after administration compared to *Lis1*$^{+/-}$, with **P $<$ 0.01. Error bars in graphs were expressed as mean ± SEM. (a, d) SNJ1945 was taken orally as a mixture with food by pregnant dams at E12.5 (200 μg/g). At the indicated time, fetal brains were dissected and subjected to Western blotting analysis. We analyzed ten independent fetuses, and obtained reproducible results. One representative data set is shown. (b, e) SNJ1945 was gavage fed orally as a mixture with 0.5% carboxymethyl cellulose to neonatal pups (200 μg/g). At indicated time, brains of neonatal pups were dissected and subjected to Western blotting analysis. We analyzed ten independent pups. (c, f) SNJ1945 was taken orally as a mixture with food by *Lis1*$^{+/-}$ mice at three weeks after birth (200 μg/g). At indicated time, brain was dissected and subjected to Western blotting analysis. We analyzed ten independent mice, and obtained reproducible results. Note: LIS1 levels were increased to normal levels by 12 hrs. after oral administration. Importantly, SNJ1945 was effective in mice at three weeks, indicating that SNJ1945 is able to pass the BBB and protect LIS1 from degradation.

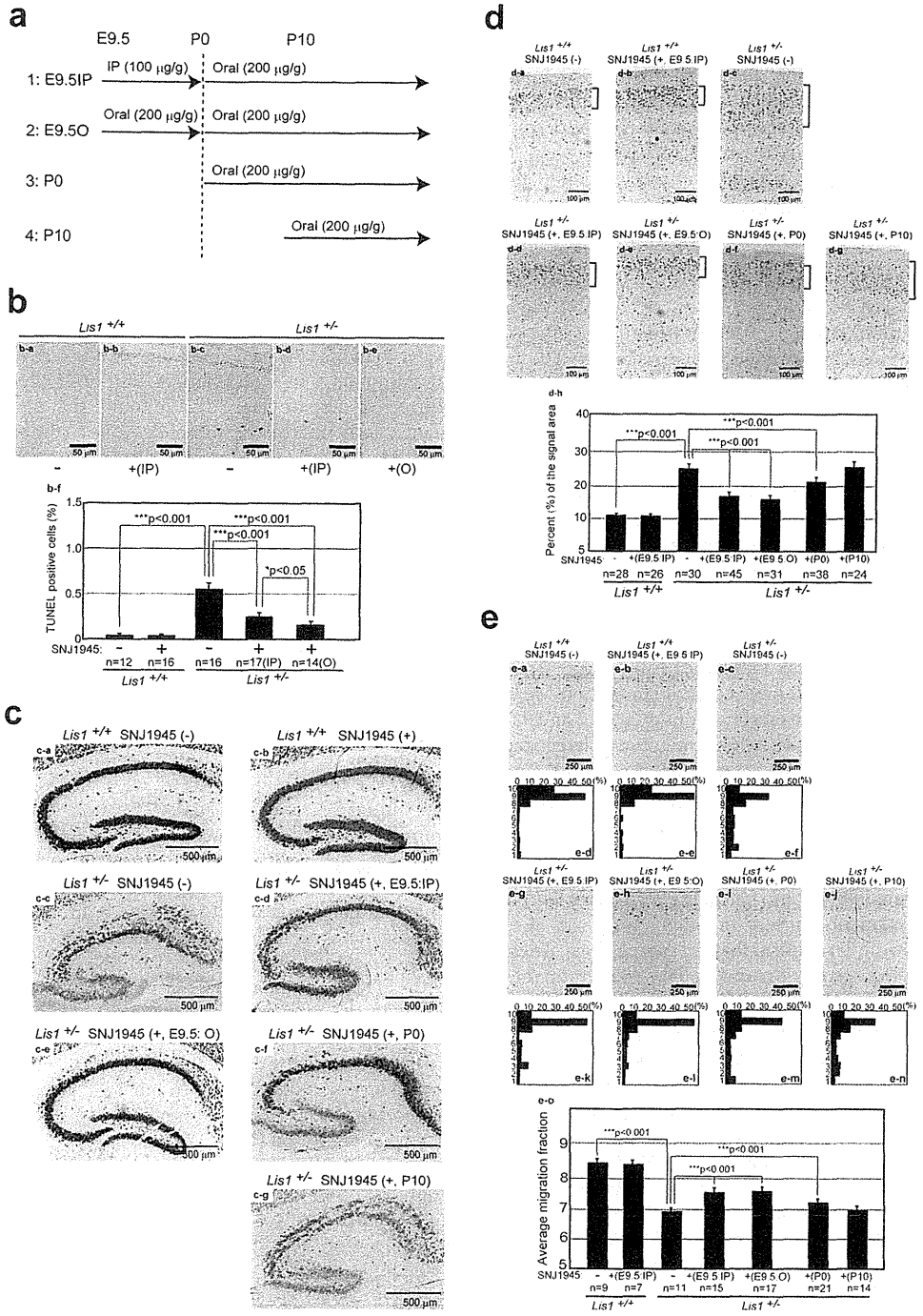


**Figure 2 | Rescue of defective corticogenesis in *Lis1*$^{+/-}$ mice by SNJ1945.** (a) Administration of SNJ1945 via four protocols (see methods). (b) Apoptotic cell death was examined by TUNEL staining at E15.5. One representative data set is shown (b-a, b, c, d, e). Histogram plots of the relative frequency of TUNEL positive cells to the total number of cells are shown at the bottom (b-f). The staining patterns are representative of different experiments as indicated at the bottom of the panel. *n* is the number of examined brains. Statistical examination was performed by unpaired Student's *t*-test. Error bars in graphs were expressed as mean ± SEM. (c) Neu-N staining of mid-sagittal sections of the hippocampus is shown. Severe cell dispersion and splitting of CA3 region were observed in the *Lis1*$^{+/-}$ mouse hippocampus (c-c), which improved by the administration of SNJ1945 (c-d, e, f, g). Other examples are shown in Supplementary Figure 6. (d) Cortical phenotypes were examined using a layer specific maker, Brn-1 (layer 2 and 3). The distribution of Brn-1 positive cells is indicated at the right side of each panel (d-a, b, c, d, e, f, g). Brn-1 positive cells were more dispersed in the *Lis1*$^{+/-}$ mouse (d-c). Quantitation of the thickness of Brn-1 positive cells is summarized at the bottom (d-h). The staining patterns are representative of different experiments as indicated at the bottom of the panel. The dispersion of Brn-1 positive cells is improved by the administration of SNJ1945. *n* is the number of examined brains. Statistical examination was performed by unpaired Student's *t*-test. Values in graphs were expressed as mean ± SEM. (e) BrdU birthdating analysis revealed neuronal migration defects in the *Lis1*$^{+/-}$ mouse. Quantitation of the thickness of BrdU positive cells is summarized at the bottom (e-o). The distribution of BrdU labeled cells in each bin that was equally divided the cortex from ML to SP. The staining patterns are representative of five different experiments. The shift downward toward the ventricular side as *Lis1* was disrupted. Treatment of SNJ1945 rescued neuronal migration to more superficial (later born and further migrating) areas.

administration after birth (200 μg/g), (2) oral administration starting at E9.5 (200 μg/g) followed by oral administration after birth (200 μg/g), (3) oral administration starting in the peri-natal period (200 μg/g) and (4) oral administration starting ten days after birth (200 μg/g). We previously reported a mild reduction of the density of cells in the neocortex of the *Lis1*$^{+/-}$ mice[11]. At E15.5 when later migrating neurons are generated, a significant acceleration of apoptotic cell death in the ventricular zone was observed[11]. These results prompted us to investigate apoptotic cell death during corticogenesis by TUNEL staining at E15.5 (Fig. 2b). In *Lis1*$^{+/-}$ mice, apoptotic cell death was clearly increased[11]. In contrast, administration of SNJ1945 suppressed apoptotic cell death in *Lis1*$^{+/-}$ mice (Fig. 2b). We also examined whether administration of SNJ1945 had any effects on mitotis, since LIS1 is essential for mitotic cell division[12] and neuroepithelial stem cell proliferation[13]. At E13.5, we performed BrdU pulse labeling and found that BrdU incorporation was not significantly different among the five groups (Supplementary Fig. 5), indicating that there was no measureable effect of SNJ1945 on proliferation of neuroepithelial stem cells. We next examined the effect of SNJ1945 on the cortical and hippocampal layering of neurons. *Lis1*$^{+/-}$ mice exhibited laminar splitting and discontinuities of pyramidal cells in the CA3 and CA2 region of the hippocampus (Fig. 2c), as we previously demonstrated[12]. After administration of SNJ1945 *in utero*, *Lis1*$^{+/-}$ mice also displayed splitting and discontinuities in the pyramidal cell layer of the hippocampus, but these defects were markedly improved compared with untreated mice (Fig. 2c and Supplementary Fig. 6a–c). To examine cortical lamination, we analyzed Brn-1 immunoreactivity, to label neurons of layer 2 and 3[14]. In *Lis1*$^{+/-}$ mice, Brn-1 positive cells (which migrate at later stages) exhibited a broader distribution compared to *Lis1*$^{+/+}$ mice. Administration of SNJ1945 resulted in more tightly packed layer 2/3 neurons in *Lis1*$^{+/-}$ mice (Fig. 2d), suggesting that neuronal migration in the cortex was also improved by the inhibition of LIS1 degradation. In both the hippocampus and cortex, oral administration starting postnatally was also partially effective but less effective than when treatment started *in utero* (Fig. 2c, d and Supplementary Fig. 6a–c). To confirm that the morphological defects observed in *Lis1*$^{+/-}$ mice were improved by SNJ1945 treatment, we performed quantitative BrdU birthdating analysis. In *Lis1*$^{+/-}$ mice, the distribution of labeled cells was shifted downward toward the ventricular zone in the cortex, and BrdU-labeling was more diffusely localized (Fig. 2e), as we previously demonstrated[12]. These migration defects associated with the disruption of *Lis1* were partially rescued in the presence of SNJ1945 (Fig. 2e). Thus, we concluded that oral administration or intra-peritoneal injection of SNJ1945 *in utero* are effective in rescuing defective neuronal migration. Importantly, oral administration commencing postnatally was also partially effective, resulting in improvement of brains structure including hippocampus and cortex. In contrast, oral administration starting ten days after birth did not result in any obvious benefits, suggesting that some fraction of neurons was still migrating at the time of birth[15], which was essentially complete by ten days after birth.

**SNJ 1945 partially rescued impaired motor behavior.** *Lis1*$^{+/-}$ mice displayed abnormal behavior and impaired spatial learning[7,16]. Therefore, we examined whether administration of SNJ1945 to *Lis1*$^{+/-}$ mice is effective in improving motor behavior compared to untreated *Lis1*$^{+/-}$ mice. Body weight and temperature were not significantly different among groups, (Supplementary Table 1). As shown in our previous report, *Lis1*$^{+/-}$ mice exhibited shorter wire-hang latency compared with wild-type mice, and this decreased latency was rescued by SNJ1945 treatment (Fig. 3a). This improvement was most significant in the group in which treatment was started from fetal times (*Lis1*$^{+/-}$E9.5). Next, we examined rotarod performance. The latency to fall for the SNJ1945-minus group was significantly less than wild type mice, as we previously reported[7]. Impaired performance on the rotarod test was significantly improved in the SNJ1945-treated groups (Fig. 3b, Supplementary Fig. 7). This functional improvement was also observed not only in the *Lis1*$^{+/-}$E9.5 group, but also in the *Lis1*$^{+/-}$P0 group, in which treatment was started perinatally. In our previous report, we demonstrated that *in utero* treatment of a calpain inhibitor from fetal stages improved gait performance. Consistent with this finding, administration of SNJ-1945 significantly improved the percent of stride in swing and swing to stance ratios in the *Lis1*$^{+/-}$E9.5 group (Fig. 3c). Most importantly, these improvements were also observed in the *Lis1*$^{+/-}$P0 and *Lis1*$^{+/-}$P10 groups. The Porsolt forced swim test is the most commonly used test for assessment of depression-like behavior in animal models. Mice were placed in an inescapable cylinder half-filled with water to induce the behavioral state of despair. We measured periods of immobility, in which longer immobile times indicated higher degrees of despair (Fig. 3d). We found that *Lis1*$^{+/-}$ mice displayed significantly increased immobile times compared with controls. SNJ1945 treated *Lis1*$^{+/-}$ groups displayed immobile times intermediate between *Lis1*$^{+/+}$ mice and *Lis1*$^{+/-}$ mice. In particular, improvement close to normal levels was observed in the *Lis1*$^{+/-}$E9.5 group. Our findings suggest that SNJ1945 treatment can rescue depression-like status in *Lis1*$^{+/-}$ mice. It is possible that the rescue of this behavioral abnormalities in *Lis1*$^{+/-}$ mice by SNJ1945 treatment results from the improved coordination of motor function by SNJ1945. Another possibility is that treatment of SNJ1945 rescued depression-like status in *Lis1*$^{+/-}$ mice, which led to improvement of behavioral performance.

**Small-animal positron emission tomography (PET) was used for evaluation of brain functional improvement by SNJ1945 treatment.** We further addressed whether the rescue of defective behaviors in *Lis1*$^{+/-}$ mice by SNJ1945 treatment was associated with the improvement of brain function. Small-animal imaging studies using PET have been increasingly applied in murine models for drug discovery[1]. We here employed PET imaging with 2-deoxy-2-$^{18}$F-fluoro-D-glucose (FDG) to evaluate brain neural activity based on glucose metabolism[17]. We found aberrations in FDG uptake patterns in *Lis1*$^{+/-}$ mice that responded to SNJ1945 treatment. PET scans with FDG in human lissencephaly patients demonstrated two layers in the cerebral cortex that could be differentiated based on metabolic activity[18], corresponding to the inner cellular layer of the lissencephalic cortex and the molecular, outer cellular, and cell-sparse layers, respectively[18]. In our PET imaging, we were not able to observe such a layered pattern in *Lis1*$^{+/-}$ mice due to the limitation of spatial resolution (Fig. 4a). *Lis1*$^{+/-}$ mice displayed similar glucose utilization in the cortex, hippocampus and cerebellum compared to wild type mice (Supplementary Fig. 8). Interestingly, we found significantly reduced glucose utilization in the basal forebrain, hypothalamus and amygdala (Fig. 4a, b). Most importantly, these reductions in FDG uptake were reversed by the treatment with SNJ1945 (Fig. 4a, b). The recovery of glucose metabolism is consistent with the improvement of behavioral performance by treatment with SNJ1945.

**SNJ1945 improved neural network formation and facilitated clustering of GABA receptors in amygdala.** Because behaviors and brain metabolism are highly linked to the interactive dynamics of neural circuits and synaptic formation in the brain, it is possible that SNJ1945 also rescued defective network formation and synaptogenesis in *Lis1*$^{+/-}$ mice, which might account for the functional improvement of behavioral performance and FDG uptake even without migratory rescue (such as after treatment commencing at P10). To address this question, we injected *TdTomato*[19] into embryos to visualize neural networks at E16.5[20]. In particular, we have focused on neural networks in amygdala (Fig. 5a). While there were no notable differences in the size of the soma, *Lis1*$^{+/-}$ mice displayed a striking simplification of dendrites compared to *Lis1*$^{+/+}$ mice

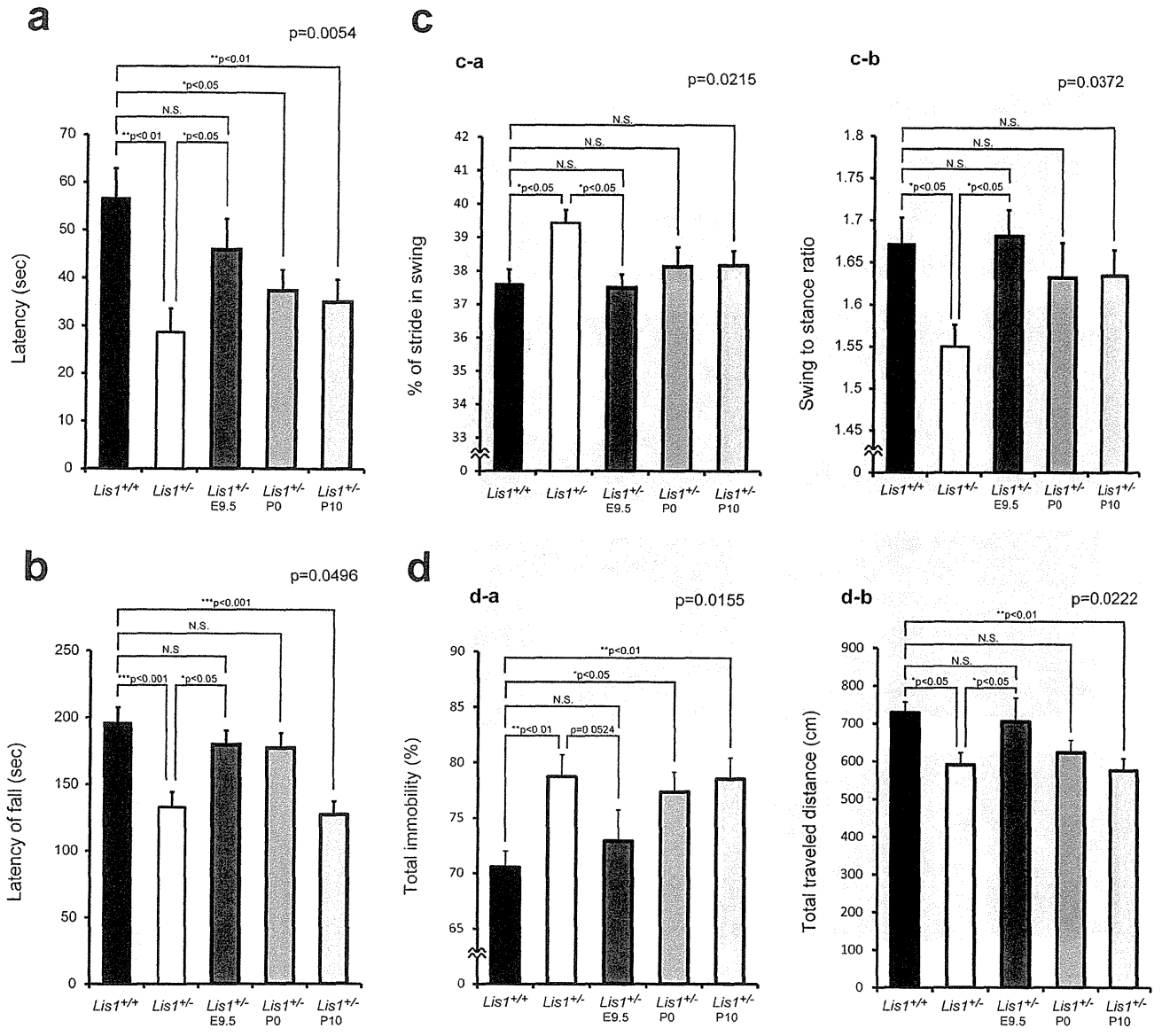


**Figure 3 | Mouse behavior analysis.** We examined behavioral performance of $Lis1^{+/+}$ mice, $Lis1^{+/-}$ mice and $Lis1^{+/-}$ mice with SNJ1945 treatment after the administration protocol described in Fig. 2a. $Lis1^{+/+}$, wild type mice, $Lis1^{+/-}$; $Lis1^{+/-}$ mice without treatment, $Lis1^{+/-}$E9.5; $Lis1^{+/-}$ mice with oral administration from E9.5 (200 μg/g) followed by oral administration after birth (200 μg/g), $Lis1^{+/-}$P0; $Lis1^{+/-}$ mice with oral administration from peri-natal period (200 μg/g) $Lis1^{+/-}$P10; $Lis1^{+/-}$ mice with oral administration from ten days after birth (200 μg/g). P-values are shown at the upper parts of bars. Statistical analysis was conducted using Stat View (SAS institute). Data were analyzed by one-way ANOVA. Error bars in graphs were expressed as mean ± SEM, and P-values indicated a group effect by one-way ANOVA. Statistical significance was defined as $^{*}P < 0.05$, $^{**}P < 0.01$ and $^{***}P < 0.001$. (a) Wire hang test. $Lis1^{+/-}$ mice displayed clear shorter latency to fall in the wire hang test. Administration of SNJ1945 improved hanging time. (b) Examination of motor function by the rotarod test. Time spent balanced on top of the rotating rod was measured across six test trials. The graph indicates summation of the latency through the six test trials. Significant differences between $Lis1^{+/+}$ mice and $Lis1^{+/-}$ mice ($^{***}P < 0.001$) were observed. SNJ1945 treatment resulted in improvement of rotarod performance but was less effective with the delayed treatment. Importantly, treatment starting at P0 was still effective. (c) Gait analysis using the DigiGait treadmill apparatus: percent of stride in swing (c-a) and swing to stance ratio (c-b) are shown. $Lis1^{+/-}$ mice with SNJ1945 treatment displayed improvement of gait parameters. Importantly, treatment from P10 was still effective, suggesting SNJ1945 can improve brain function after much of development has finished. (d) Porsolt swimming test. Immobility (d-a) and distance traveled (d-b) are shown at Day 2.

(Fig. 5b, c, d, Supplementary Fig. 9). Branching and length of each branch were decreased to approximately 29% and 27%, respectively. Importantly, the poor development of dendritic arbors and decreased each length in $Lis1^{+/-}$ mice were rescued by SNJ1945 treatment (Fig. 5b, c, d, Supplementary Fig. 9), suggesting that neurons in the amygdala partially maintain plasticity, and proper network formation was facilitated by the treatment after P10.

The amygdala has an important role in processing emotional information[21–23]. Inappropriate processing within the amygdala is thought to induce anxiety disorders. Benzodiazepines, which act specifically on $GABA_A$ receptors, are commonly used as anxiolytics. This implies that GABAergic synapses within the amygdala may have an important role in inducing or compensating for these disorders. $GABA_A$ receptors are clustered at synaptic sites to achieve a

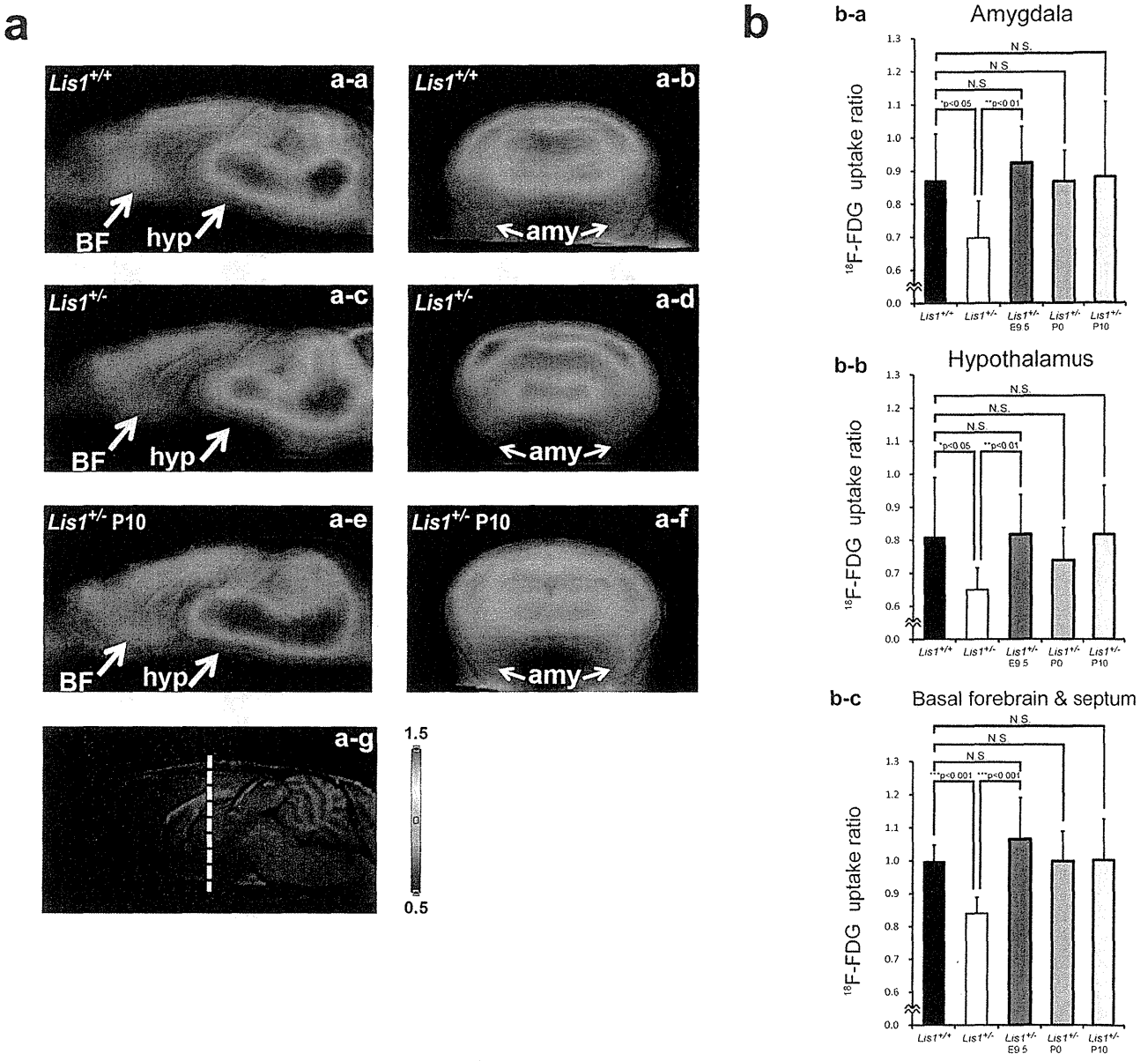


**Figure 4 | Brain metabolism: $^{18}$F-FDG PET scanning.** *In vivo* $^{18}$F-FDG-PET images and surface renderings of wild type (WT) mice and *Lis1*$^{+/-}$ mice are depicted. (a) Co-registration of microPET and MRI images obtained from WT mice (a-a, b) or *Lis1*$^{+/-}$ mice (a-c, d, e, f). The basal forebrain and hypothalamus are indicated by white arrows in sagittal images (BF, basal forebrain; hyp, hypothalamus) and amygdala is indicated by white arrows in coronal images (amy, amygdala). The location of coronal slice images is indicated as a white dash line in the sagittal MR image (a-g). Graded 2D slice images demonstrate the reduction of $^{18}$F-FDG uptake in the basal forebrain, hypothalamus and amygdala of *Lis1*$^{+/-}$ mice (a-c, d). The color bar indicates normalized $^{18}$F-FDG uptake ratio. (b) Quantification of $^{18}$F-FDG uptake in several brain regions of each experimental group (*Lis1*$^{+/+}$; *Lis1*$^{+/+}$ mice without treatment (n = 8), *Lis1*$^{+/-}$; *Lis1*$^{+/-}$ mice without treatment (n = 8), *Lis1*$^{+/-}$E9.5; *Lis1*$^{+/-}$ mice with SNJ1945 treatment from E9.5 (n = 6), *Lis1*$^{+/-}$P0; *Lis1*$^{+/-}$ mice with SNJ1945 treatment from peri-natal period (n = 7) *Lis1*$^{+/-}$P10; Lis1$^{+/-}$ mice with SNJ1945 treatment from ten days after birth (n = 6)). Statistical examination was performed by unpaired Student's *t*-test. Values in graphs were expressed as mean ± SEM. Statistical significance was defined as *P < 0.05, **P < 0.01 and ***P < 0.001.

high density of postsynaptic receptors opposite the input axonal terminals. This allows for an efficient propagation of GABA mediated signals, which mostly result in neuronal inhibition. A key organizer for $GABA_A$ receptors is gephyrin that forms oligomeric superstructures beneath the synaptic area[24,25]. In addition, gephyrin plays a crucial role in synaptic dynamics and is a platform for multiple protein-protein interactions and bringing receptors. Thus, we examined the distribution of gephyrin as an indicator for functional $GABA_A$ receptors in amygdala[26]. In *Lis1*$^{+/+}$ mice, somata and proximal dendrites of amygdala neurons exhibited a variety of gephyrin clusters from very small round puncta to large and bright clusters (Fig. 5b). While *Lis1*$^{+/-}$ mice displayed similar pattern of gephyrin clusters with *Lis1*$^{+/+}$ mice, they were significantly decreased (Fig. 5b, e). Decreased gephyrin clusters in *Lis1*$^{+/-}$ mice were rescued by SNJ1945 treatment commencing at P10 (Fig. 5b, e). Thus, we concluded that post-natal treatment of SNJ1945 was effective for recovery of defective network formation and decreased receptor distribution in amygdala.

**SNJ1945 augmented retrograde transport of nerve growth factor (NGF) in dorsal root ganglia (DRG) neurons.** Neural growth

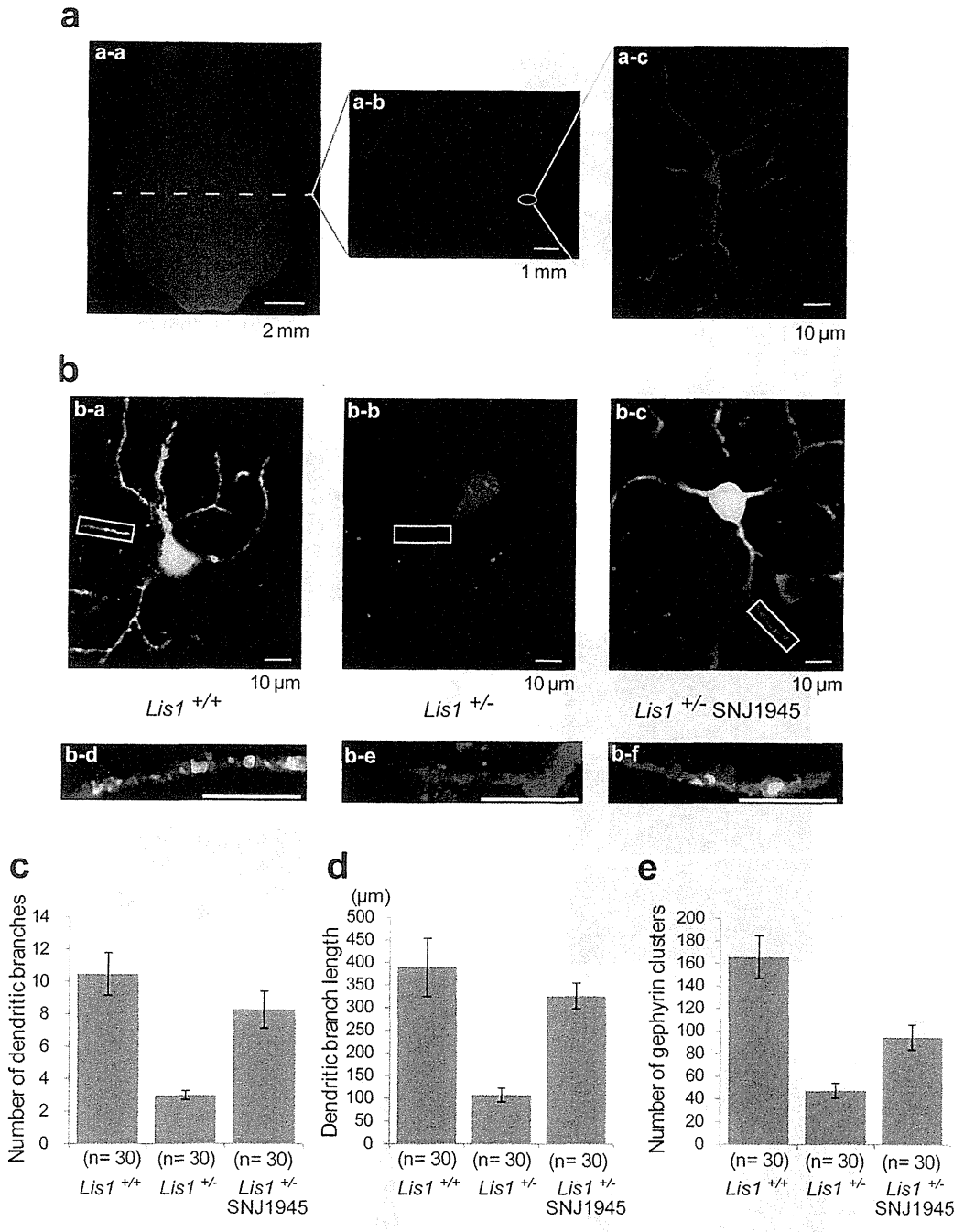


**Figure 5 | Examination of neuronal networks and clustering of GABA receptors.** (a) Neural fibers were visualized by the expression of TdTomato through *in utero* gene transfer. Ventral view image of whole brain by fluorescence dissecting microscope (a-a), confocal images at low (a-b) and high magnifications of representative fields (a-c) from coronal amygdala (white circle) are shown. (b) Individual image of amygdala neurons. Neural fiber was visualized by the TdTomato expression (red), which was decorated by gephyrin clusters (green). Representative images from $Lis1^{+/+}$ mice (b-a, d), $Lis1^{+/-}$ mice (b-b, e) and $Lis1^{+/-}$ mice with P10 treatment (b-c, f) are shown. Note: $Lis1^{+/-}$ mice exhibited poor arbors of neural fiber and decreased clusters of gephyrin, which were rescued by the treatment of SNJ1945. We examined five independent transfected brains for each, which were subjected to serial cryostat section with 5 μm thickness. Statistical examination of branching frequency (c), total length of branches (d) and number of gephyrin clusters (e) was performed.

factors are crucially important for activity-dependent plastic changes in synaptic strength and network refinement. We assumed that the SNJ1945 dependent rescue of neural network formation and receptor distribution might be attributable to the recovery of retrograde transport of neural growth factors. Retrograde axonal transport of nerve growth factor (NGF) signals is critical for the survival, differentiation, and maintenance of peripheral sympathetic and sensory neurons and basal forebrain cholinergic neurons. To examine retrograde transport of NGF, we used quantum dots (Qd-NGF) to track retrograde transport of NGF in cultures of mouse DRG neurons. Using pseudoTIRF microscopy, we tracked the movement of Qd-NGF in live DRG neurons in real time[27]. We applied non-compartmentalized cultures of DRG neurons, which displayed both directional movements of Qd-NGFs. Live-cell

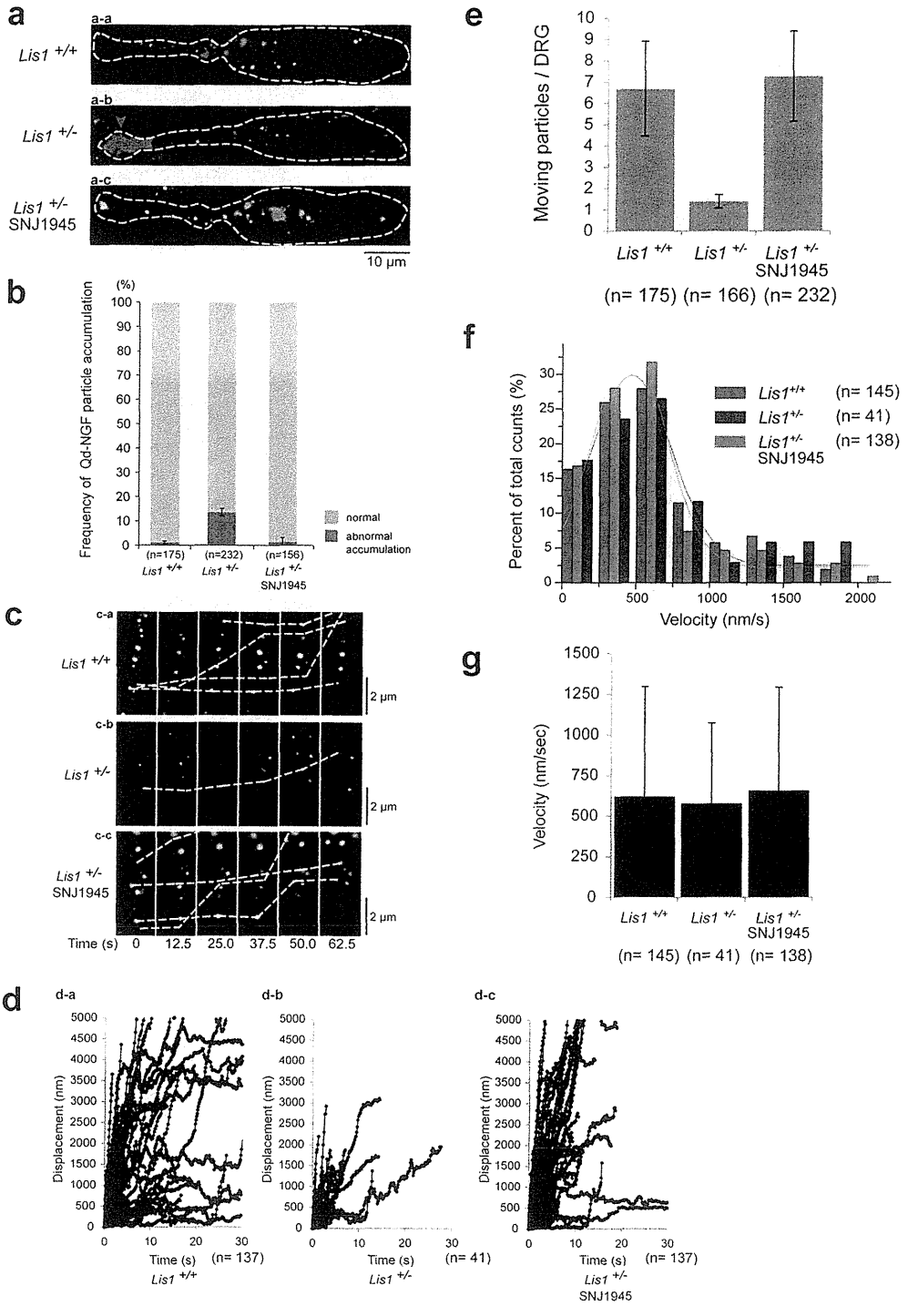


**Figure 6 | Retrograde transport of NGF in DRG neurons.** To show that the Qd-NGF complex can be internalized at axon terminals and transported in a retrograde fashion to neuron cell bodies, quantum dots were conjugated to NGF (Qd-NGF) and incubated with DRG neurons followed by pseudoTIRF microscope examination. (a) Qd-NGF were internalized and transported to the cell body. White dotted line indicates the contour of DRG neurons. DRG neurons from *Lis1*$^{+/+}$ mice (a-a), *Lis1*$^{+/-}$ mice (a-b) and *Lis1*$^{+/-}$ mice with P10 treatment (a-c) are shown. Note: in *Lis1*$^{+/-}$ mice, Qd-NGF dots were internalized, but aberrantly accumulated at the tips of DRG neurons (red arrowhead). (b) Each percentage of abnormal accumulation was presented as mean ± SEM. n indicates the number of examined DRG neurons. Aberrant accumulation was exclusively observed in in *Lis1*$^{+/-}$ mice, which was rescued by SNJ1945 treatment. (c) Transport dynamics of Qd-NGF containing endosomes. Time-lapse video images of endosomes are shown. Lapsed time is shown at the bottom of panel. Retrograde transport of Qd-NGF containing endosomes in *Lis1*$^{+/-}$ mice was decreased (c-b). (d) Trajectories of endosomes from *Lis1*$^{+/+}$ mice (d-a), *Lis1*$^{+/-}$ mice (d-b) and *Lis1*$^{+/-}$ mice with P10 treatment (d-c) are shown. (e) Number of transported endosomes per DRG neuron was presented as mean ± SEM. n indicates the number of examined DRG neurons. Note: We found that significant reduction of the frequency in *Lis1*$^{+/-}$ mice, which was rescued by SNJ1945 treatment. (f) Histograms of velocities of retrograde-directed endosomes. (g) Mean velocities are 0.62 μm/s in *Lis1*$^{+/+}$ mice, 0.60 μm/s in *Lis1*$^{+/-}$ mice and 0.65 μm/s in *Lis1*$^{+/-}$ mice with P10 treatment. There was no significant difference in each group.

imaging revealed that Qd-NGFs were internalized at axon terminals and transported in a retrograde fashion to cell bodies in DRG neurons from *Lis1*$^{+/+}$ mice (Supplementary movie 1). Importantly, Qd-NGFs were internalized, but accumulate aberrantly at tips of DRG neurons from *Lis1*$^{+/-}$ mice (Fig. 6a, b). This aberrant accumulation was rescued by treatment of SNJ1945 (Fig. 6a, b). Our observations were similar with transport defects peroxisomes and endosomes in the genetic absence of *Lis1/nudF* of filamentous fungus *Aspergillus nidulans*[28]. Next, we characterized the transport of Qd-NGF containing endosomes. Kymographs from time-lapse videos of Qd-NGFs indicated that the retrograde transport of Qd-NGF containing endosomes moved in a stop-and-go manner (Fig. 6c, d, Supplementary movie 1). Strikingly, we found that the frequency of retrograde transport of Qd-NGF containing endosomes was significantly decreased in DRG neurons from *Lis1*$^{+/-}$ mice (Fig. 6c, d, e, Supplementary movie 2), whereas the frequency of anterograde transport of Qd-NGF containing endosomes was not affected (Supplementary Fig. 9). In clear contrast, the velocity of retrograde transport of Qd-NGF containing endosomes was intact in DRG neurons from *Lis1*$^{+/-}$ mice (Fig. 6f, g), which was also consistent with *Aspergillus nidulans*[28]. We next examined the effect of SNJ1945 in the decreased frequency of the retrograde transport. Importantly, the treatment of SNJ1945 clearly recovered the defective retrograde transport of Qd-NGF containing endosomes (Fig. 6c, d, e, Supplementary movie 3). Presumably, the protection of LIS1 degradation by SNJ1945 restored proper dynein distribution, resulting in the recovery of retrograde transport of Qd-NGF containing endosomes, which may stimulate network formation and receptor distribution.

## Discussion

SNJ1945 is permeable to the BBB, and was effective in rescuing defects in *Lis1*$^{+/-}$ mice after treatment commenced perinatally. These findings suggest that SNJ1945 may be considered for the treatment of lissencephaly patients postnatally. In support of this, we demonstrated that SNJ1945 improved behavioral performances and brain glucose metabolism after treatment ten days after birth without histological rescue of brain disorganization. We also demonstrated that SNJ1945 stimulated network formation and receptor distribution, explaining functional rescue by SNJ1945. These functional rescues are partially attributable to restoration of growth signal, characterized by the recovery of retrograde transport of Qd-NGF containing endosomes. These findings support a potential therapeutic approach with a novel calpain inhibitor, SNJ1945, in the human ILS patient that has a *LIS1* mutation.

## Methods

**BrdU birthdating and proliferation studies.** All mouse experiments were performed under the approval from the experimental animal committee of Osaka City University Graduate School of Medicine or the approval of the experimental animal committee of Osaka City University Graduate School of Medicine, National Institute for Physiological Sciences and Fujita Health University.

For bromodeoxyuridine (BrdU) experiments, pregnant dams (E15.5) were injected with BrdU (50 μg/g, i.p.), and the distribution of BrdU-positive cells was determined at P5. For pulse labeling to examine proliferation of neuroepithelial stem cell, pregnant dams (E13.5) were injected with BrdU (150 μg/g, i.p.). Subsequently, the distribution of BrdU-positive cells was determined one hour after injection. The incorporation of BrdU in cells was detected with a mouse anti-BrdU monoclonal primary antibody (Roche) followed by an alkaline phosphatase-conjugated secondary antibody (Boehringer Mannheim). We analyzed three independent mice for each genotype.

**Histological examination and immunohistochemistry.** After perfusion with 4%PFA fixative, tissues from wild type and mutant mice were embedded in paraffin and sectioned at 5 μm thickness. After deparaffination, endogenous peroxidase activity was blocked by incubating the sections in 1.5% peroxide in methanol for 20 min. The sections were then boiled in 0.01 M/liter citrate buffer, pH 6.0, for 20 min and cooled slowly. Before staining, the sections were blocked with rodent block (LabVision) for 60 min. The sections were washed in PBS and incubated with an anti-Brn-1 antibody (Santa Cruz).

**Cell culture and immunocytochemistry.** Human fibroblasts were grown in D-MEM supplemented with 10% FBS. To inhibit calpain, cells were incubated with 200 μM SNJ1945 or control DMSO for 2 hrs. Cells were fixed in 4% PFA in PBS followed by permealization with 0.2% Triton X-100 in PBS. Coverslips were blocked for one hour with Block Ace (Yukijirushi) in PBS supplemented with 5% BSA, and were incubated for 1 hr in primary antibody, washed, and incubated for 1 hr using Alexa 546-conjugated secondary antibodies (Molecular Probes). Primary antibodies were an anti-βCOP antibody (Sigma) and an anti-DIC1 antibody (Chemicon).

**Behavioral analysis.** *Lis1*$^{+/+}$ mice and *Lis1*$^{+/-}$ mice that were treated with and without SNJ1945 were used for behavioral experiments, as described in the figure legend for Figure 2a. *Lis1*$^{+/-}$ mice had a single *Lis1* mutant allele. In this study mice were on an FVB background. All behavioral tests were carried out with male mice that were at least 9 weeks old at the start of testing. Raw data from the behavioral tests, the date on which each experiment was performed, and the age of the mice at the time of the experiment are shown in the mouse phenotype database (http://www.mouse-phenotype.org/). Mice were group-housed (four mice per cage) in a room with a 12 h light/dark cycle (lights on at 7:00 a.m.) with access to food and water *ad libitum*. The room temperature was kept at 23 ± 2°C. Behavioral testing was performed between 9:00 a.m. and 6:00 p.m. After the tests, all apparatus were cleaned with diluted sodium hypochlorite solution to prevent a bias due to olfactory cues. Three independent groups of mice were prepared for behavioral tests. One group consisted of equal numbers of mice. *Lis1*$^{+/+}$; *Lis1*$^{+/+}$ mice without treatment, *Lis1*$^{+/-}$; *Lis1*$^{+/-}$ mice without treatment, *Lis1*$^{+/-}$E9.5; *Lis1*$^{+/-}$ mice with oral administration from from E9.5 (200 μg/g) followed by oral administration after birth (200 μg/g), *Lis1*$^{+/-}$P0; *Lis1*$^{+/-}$ mice with oral administration from peri-natal period (200 μg/g) *Lis1*$^{+/-}$P10; *Lis1*$^{+/-}$ mice with oral administration from ten days after birth (200 μg/g). Experiments were done in the following sequences; the first group (12 each): the general health and neurological screen including wire hang test (GHNS), light/dark transition (LD), rotarod (RR) and gait analysis (GA); the second group (16 each): GHNS, LD, RR and GA; the third group (24 each): GHNS, LD, open field (OF), elevated plus maze (EP), hot plate (HP), one-chamber social interaction test (SI), RR, Crawley's sociability and preference for social novelty test (CSI), startle response/prepulse inhibition test (PPI), Porsolt forced swim test (PS), fear conditioning test (FZ), tail suspension test (TS), and social interaction test in home cage (HC-SI). Behavioral data were obtained automatically by applications based on the public domain Image J program and modified for each test by Tsuyoshi Miyakawa (available through O'HARA & CO., Tokyo, Japan)[29]. Each behavioral test was separated from each other at least by 1 day.

Briefly, the rotarod test, using an accelerating rotarod (UGO Basile Accelerating Rotarod), was performed by placing mice on rotating drums (3 cm diameter) and measuring the time each animal was able to maintain its balance on the rod. The speed of the rotarod accelerated from 4 to 40 rpm over a 5-min period. Gait analysis was performed using ventral plane videography as described. Mice were placed on the treadmill belt that moves at a speed of 24.7 cm/s. Digital video images of the underside of mice were collected at 150 frames per second. The paw area indicates the temporal placement of the paw relative to the treadmill belt. The color images were converted to their binary matrix equivalents, and the areas (in pixels) of the approaching or retreating paws relative to the belt and camera were calculated throughout each stride. Plotting the area of each digital paw print (paw contact area) imaged sequentially in time provides a dynamic gait signal, representing the temporal record of paw placement relative to the treadmill belt. For Porsolt forced swimming test, the apparatus consisted of four plastic cylinders (20 cm height × 10 cm diameter). The cylinders were filled with water (23°C) up to a height of 7.5 cm. Mice were placed into the cylinders, and their behavior recorded over a 10-min test period. Data acquisition and analysis were performed automatically, using Image PS software (see above). All behavioral testing procedures were approved by the Animal Care and Use Committee of National Institute for Physiological Sciences and Fujita Health University.

**MicroPET scan and data analysis.** PET imaging data were obtained in male mice (20–30 g) using a small animal PET camera (microPET Focus-220, Simens Medical Systems), which has a transaxial resolution of 1.4 mm in full width at half-maximum. Data were acquired in a 128 × 128 × 95 matrix with a pixel of 0.475 mm and a slice thickness of 0.796 mm. Before PET scanning, mice were intravenously injected with $^{18}$F-FDG (approximately 0.5 MBq/g B.W.) through a cannula inserted into the tail vein and were kept in their home cage for 30 min for the $^{18}$F-FDG uptake under freely moving condition. Subsequently, the mice were placed in the small-animal PET scanner under isoflurane anesthesia (4% for induction and 1.5% for maintenance) with $O_2$ and $N_2O$ gas. Static acquisitions were performed during 30 min. PET images were reconstructed using a filtered backprojection (FBP) algorithm. The image data acquired from microPET were analyzed by ASIPro VM (ver. 6.0, Concorde Microsystems Inc.) and PMOD (ver. 3.4, PMOD Technologies Ltd.) software. The PET and magnetic resonance (MR) images were co-registered using a PMOD software. MR images were obtained from *Lis1*$^{+/+}$ mice and *Lis1*$^{+/-}$ mice used for the PET study under isoflurane anesthesia with a 7 tesla MR scanner (BioSpec 70/20, Bruker). Volumetric regions of interest were placed on the several brain regions (striatum, cerebral cortex, hippocampus, thalamus, cerebellum, hypothalamus, amygdala, basal forebrain and septum, brain stem, midbrain, superior colliculi) based on the MR images. Relative regional $^{18}$F-FDG uptake was determined by normalized count data to those in the whole brain. Each value was presented as mean ± SEM. Statistical analysis was performed using the SPSS Statistics Student software. Data

were analyzed using one-way ANOVA followed by *post hoc* Tukey's test for comparison among groups. Significance threshold was assumed at $P < 0.05$.

***In utero* transfection.** Expression vectors were introduced into fetal brains by an *in utero* electroporation-mediated gene transfer method[20]. Briefly, pregnant mice were deeply anesthetized on E16.5, and the uterine horns were exposed. Approximately 2 μl of *TdTomato* plasmid solution was injected into the lateral ventricle from outside the uteri with a glass micropipette (GD-1.5, Narishige, Tokyo, Japan). Each embryo in the uterus was then placed between the tweezers-type electrodes described above and electronic pulses (45 V; 50 msec duration) were applied five times at intervals of 950 msec (GUY21, Bexco ltd). The uterine horns were then placed back into the abdominal cavity to allow the embryos to continue normal development. Histological examination was performed 5 days after *in utero* injection (P2-P3). Histological examination was performed 35 days after *in utero* injection (P30). SNJ1045 as applied from P10 by oral administration.

**Examination of retrograde transport of NGF by pseudoTIRF microscope and live imaging.** NGF was conjugated with Qd655 via carboxyl group substitution by using the coupling reagent 1-ethyl-3-(3-dimethylaminopropyl) -carbodiimide (EDAC) (Pierce Biotech, Rockford, IL). An inverted microscope (Olympus 1 × 71) was modified for pseudoTIRF illumination. The laser beam (488 nm) was focused at the back focal plane of the objective lens (ApoN×60, 1.49 Oil, Olympus). The incident angle was adjusted to be slightly smaller than the critical angle so that the laser beam could penetrate ≈1 μm into the aqueous solution. To image transport of Qd-NGF in live neurons, DRG neurons were incubated with Qd-NGF. Fluorescence images were filtered with a Qd655/15 emission filter. Time-lapse images were acquired by using an EMCCD camera (ImageM, Hamamatsu photonics) at the speed of 5–10 frames per second.

**LC-MS/MS analysis.** The SNJ1945 concentration in the brain was determined by turbo ion spray on an API 4000 triple-quadrupole mass spectrometer (Applied Biosystems) equipped with a turbo ion spray source using multiple reaction monitoring (MRM). Chromatography was performed on a NANOSPACE SI-2 HPLC system (Shiseido) with Shiseido Capcell pak C18 MG-II column. The extraction of SNJ1945 from the brain and the measuring condition were described in the literature[9].


1. Beckmann, N. *et al.* In vivo mouse imaging and spectroscopy in drug discovery. *NMR Biomed* **20**, 154–185 (2007).
2. Reiner, O. *et al.* Isolation of a Miller-Dieker lissencephaly gene containing G protein beta-subunit-like repeats. *Nature* **364**, 717–721 (1993).
3. Hattori, M., Adachi, H., Tsujimoto, M., Arai, H. & Inoue, K. Miller-Dieker lissencephaly gene encodes a subunit of brain platelet-activating factor acetylhydrolase [corrected]. *Nature* **370**, 216–218 (1994).
4. Vallee, R. B., Tai, C. & Faulkner, N. E. LIS1: cellular function of a disease-causing gene. *Trends Cell Biol* **11**, 155–160 (2001).
5. Wynshaw-Boris, A. Lissencephaly and LIS1: insights into the molecular mechanisms of neuronal migration and development. *Clin Genet* **72**, 296–304 (2007).
6. Yamada, M. *et al.* LIS1 and NDEL1 coordinate the plus-end-directed transport of cytoplasmic dynein. *Embo J* **27**, 2471–2483 (2008).
7. Yamada, M. *et al.* Inhibition of calpain increases LIS1 expression and partially rescues in vivo phenotypes in a mouse model of lissencephaly. *Nat Med* **15**, 1202–1207 (2009).
8. Koumura, A. *et al.* A novel calpain inhibitor, ((1S)-1((((1S)-1-benzyl-3-cyclopropylamino-2,3-di-oxopropyl)amino)carbonyl)-3-methylbutyl) carbamic acid 5-methoxy-3-oxapentyl ester, protects neuronal cells from cerebral ischemia-induced damage in mice. *Neuroscience* **157**, 309–318 (2008).
9. Shirasaki, Y., Yamaguchi, M. & Miyashita, H. Retinal penetration of calpain inhibitors in rats after oral administration. *J Ocul Pharmacol Ther* **22**, 417–424 (2006).
10. Oka, T. *et al.* Amelioration of retinal degeneration and proteolysis in acute ocular hypertensive rats by calpain inhibitor ((1S)-1-((((1S)-1-benzyl-3-cyclopropylamino-2,3-di-oxopropyl)amino)carbony l)-3-methylbutyl)carbamic acid 5-methoxy-3-oxapentyl ester. *Neuroscience* **141**, 2139–2145 (2006).
11. Sasaki, S. *et al.* Complete loss of Ndel1 results in neuronal migration defects and early embryonic lethality. *Mol Cell Biol* **25**, 7812–7827 (2005).
12. Hirotsune, S. *et al.* Graded reduction of Pafah1b1 (Lis1) activity results in neuronal migration defects and early embryonic lethality. *Nat Genet* **19**, 333–339 (1998).
13. Yingling, J. *et al.* Neuroepithelial stem cell proliferation requires LIS1 for precise spindle orientation and symmetric division. *Cell* **132**, 474–486 (2008).
14. McEvilly, R. J., de Diaz, M. O., Schonemann, M. D., Hooshmand, F. & Rosenfeld, M. G. Transcriptional regulation of cortical neuron migration by POU domain factors. *Science* **295**, 1528–1532 (2002).
15. Manent, J. B., Wang, Y., Chang, Y., Paramasivam, M. & LoTurco, J. J. Dcx reexpression reduces subcortical band heterotopia and seizure threshold in an animal model of neuronal migration disorder. *Nat Med* **15**, 84–90 (2009).
16. Paylor, R. *et al.* Impaired learning and motor behavior in heterozygous Pafah1b1 (Lis1) mutant mice. *Learn Mem* **6**, 521–537 (1999).
17. Mizuma, H., Shukuri, M., Hayashi, T., Watanabe, Y. & Onoe, H. Establishment of in vivo brain imaging method in conscious mice. *J Nucl Med* **51**, 1068–1075 (2010).
18. Pfund, Z. *et al.* Lissencephaly: fetal pattern of glucose metabolism on positron emission tomography? *Neurology* **55**, 1683–1688 (2000).
19. Palmer, A. E. & Tsien, R. Y. Measuring calcium signaling using genetically targetable fluorescent indicators. *Nat Protoc* **1**, 1057–1065 (2006).
20. Takitoh, T. *et al.* Activation of Aurora-A Is Essential for Neuronal Migration via Modulation of Microtubule Organization. *J Neurosci* **32**, 11050–11066 (2012).
21. Davis, M., Walker, D. L. & Myers, K. M. Role of the amygdala in fear extinction measured with potentiated startle. *Ann N Y Acad Sci* **985**, 218–232 (2003).
22. LeDoux, J. E. Emotion circuits in the brain. *Annu Rev Neurosci* **23**, 155–184 (2000).
23. Pare, D., Quirk, G. J. & Ledoux, J. E. New vistas on amygdala networks in conditioned fear. *J Neurophysiol* **92**, 1–9 (2004).
24. Takahashi, H. *et al.* Selective control of inhibitory synapse development by Slitrk3-PTPdelta trans-synaptic interaction. *Nat Neurosci* **15**, 389–398, S381–382 (2012).
25. van Versendaal, D. *et al.* Elimination of inhibitory synapses is a major component of adult ocular dominance plasticity. *Neuron* **74**, 374–383 (2012).
26. Chhatwal, J. P., Myers, K. M., Ressler, K. J. & Davis, M. Regulation of gephyrin and GABAA receptor binding within the amygdala after fear acquisition and extinction. *J Neurosci* **25**, 502–506 (2005).
27. Cui, B. *et al.* One at a time, live tracking of NGF axonal transport using quantum dots. *Proc Natl Acad Sci U S A* **104**, 13666–13671 (2007).
28. Egan, M. J., Tan, K. & Reck-Peterson, S. L. Lis1 is an initiation factor for dynein-driven organelle transport. *J Cell Biol* **197**, 971–982 (2012).
29. Yamasaki, N. *et al.* Alpha-CaMKII deficiency causes immature dentate gyrus, a novel candidate endophenotype of psychiatric disorders. *Mol Brain* **1**, 6 (2008).


## Acknowledgements


We thank Azusa Inagaki, Kaori Nakakubo, Yukimi Kira and Yoriko Yabunaka for technical support, Hiromichi Nishimura and Keiko Fujimoto for mouse breeding. This work was supported by Grant-in-Aid for Scientific Research from the Ministry of Education, Science, Sports and Culture of Japan from the Ministry of Education, Science, Sports and Culture of Japan to Shinji Hirotsune and Knowledge Cluster Initiative (Stage-2) Research Foundation to Shinji Hirotsune. This work was also supported by Takeda Science Foundation and the Sumitomo Foundation to Shinji Hirotsune and NIH grants NS41030 and HD47380 to Anthony Wynshaw-Boris. This work was also supported in part by Grant-in-Aid for Scientific Research(B) of Japan Society for the Promotion of Science (JSPS)(#22390056 to Masami Yamada), Adaptable and Seamless Technology Transfer Program (A-STEP) through Target-driven R&D, Japan Science and Technology Agency (#AS231Z02224G to Masami Yamada), Grant-in-Aid for Scientific Research on Innovative Areas of The Ministry of Education, Culture, Sports, Science and Technology (MEXT)(#11001981 to Masami Yamada) and The Uehara Memorial Foundation (to Masami Yamada). This work was also supported by KAKENHI (Grant-in-Aid for Scientific Research) on Young Scientists A (16680015), Scientific Research (B) (21300121, 21390069), Exploratory Research (19653081), Integrative Brain Research (IBR-shien), and Innovative Areas (Comprehensive Brain Science Network) from the Ministry of Education, Science, Sports and Culture of Japan (MEXT) of Japan, grant from Neuroinformatics Japan Center (NIJC), grants from CREST of Japan Science and Technology Agency (JST), and the Funding Program for Next Generation World-Leading Researchers (Next Program). This work was also supported by the Multidisciplinary program for elucidating the brain development from molecules to social behavior (Fukui Brain Project) and the Grants-in-Aid for Scientific Research and Strategic Research Program for Brain Sciences ("integrated research on neuropsychiatric disorder") by the Ministry of Education, Culture, Sports, Science and Technology of Japan to Makoto Sato. We declare no conflicts of interests.


## Author contributions

S.H. performed mouse histological examination and mouse behavioral analyasis. M.Y. performed mouse histological examination. K.T., S.H. and T.M. performed mouse behavioral analyasis (Figure 3). Y.K. and Y.T. performed PET analysis (Figure 4). K.K., Y.O., H.W. and M.S. performed neural circuit characterization (Figure 5, 6). M.A. provided us SNJ1945. K.H., M.A., K.T. and M.K. provided us a fibroblast cell line from the human lissencephaly patient. A.W.-B. and S.H. organized experiments and wrote a manuscript.

## Additional information

**Supplementary information** accompanies this paper at http://www.nature.com/scientificreports

**Competing financial interests:** The authors declare no competing financial interests.




**How to cite this article:** Toba, S. *et al.* Post-natal treatment by a blood-brain-barrier permeable calpain inhibitor, SNJ1945 rescued defective function in lissencephaly. *Sci. Rep.* 3, 1224; DOI:10.1038/srep01224 (2013).

J Cancer Res Clin Oncol
DOI 10.1007/s00432-013-1389-1

ORIGINAL PAPER

# Hepatocellular carcinoma patients with increased oxidative stress levels are prone to recurrence after curative treatment: a prospective case series study using the d-ROM test

**Yusuke Suzuki · Kenji Imai · Koji Takai · Tatsunori Hanai · Hideki Hayashi · Takafumi Naiki · Yoichi Nishigaki · Eiichi Tomita · Masahito Shimizu · Hisataka Moriwaki**

Received: 31 October 2012 / Accepted: 30 January 2013


**Abstract**
*Purpose* Oxidative stress plays an important role in liver carcinogenesis. To determine the impact of oxidative stress on the recurrence of stage I/II hepatocellular carcinoma (HCC) after curative treatment, we conducted a prospective case series analysis.
*Methods* This study included 45 consecutive patients with stage I/II HCC, who underwent curative treatment by surgical resection or radiofrequency ablation at Gifu Municipal Hospital from 2006 to 2007. In these 45 cases, recurrence-free survival was estimated using the Kaplan–Meier method. The factors contributing to HCC recurrence, including the serum levels of derivatives of reactive oxygen metabolites (d-ROM) as an index of oxidative stress, were subjected to univariate and multivariate analyses using the Cox proportional hazards model.
*Results* The serum levels of d-ROM ($P = 0.0231$), α-fetoprotein (AFP, $P = 0.0274$), and fasting plasma glucose ($P = 0.0400$) were significantly associated with HCC recurrence in the univariate analysis. Multivariate analysis showed that the serum levels of d-ROM (hazard ratio [HR] 1.0038, 95 % confidence interval [CI] 1.0002–1.0071, $P = 0.0392$) and AFP (HR 1.0002, 95 % CI 1.0000–1.0003, $P = 0.0316$) were independent predictors of HCC recurrence. Kaplan–Meier analysis showed that recurrence-free survival was low in patients with high serum d-ROM (≥570 Carr U, $P = 0.0036$) and serum AFP (≥40 ng/dL, $P = 0.0185$) levels.
*Conclusions* The serum levels of d-ROM and AFP can be used for screening patients with a high risk for HCC recurrence. Patients who show increased levels of these factors require careful surveillance.

**Keywords** Hepatocellular carcinoma · Oxidative stress · d-ROM · Carcinogenesis

## Introduction

Hepatocellular carcinoma (HCC) is one of the most common malignancies worldwide, accounting for 750,000 annual cases; approximately the same number of people (700,000) die from this malignancy each year (Jemal et al. 2011). HCC development is frequently associated with chronic inflammation and subsequent cirrhosis of the liver induced by persistent infection with hepatitis B virus (HBV) or hepatitis C virus (HCV) (El-Serag 2002). Alcohol consumption, obesity, and related metabolic disorders such as diabetes mellitus are also involved in liver carcinogenesis (El-Serag 2002). The prognosis of patients with HCC is poor because the incidence of recurrence in patients with underlying cirrhosis is very high (Toyama et al. 2008). Therefore, careful surveillance of high-risk groups for HCC and early detection before progression to an advanced stage are important to improve the prognosis of this malignancy. It is therefore a task of pressing urgency to identify useful risk factors for HCC development or recurrence. Male gender, the presence of cirrhosis,

**Electronic supplementary material** The online version of this article (doi:10.1007/s00432-013-1389-1) contains supplementary material, which is available to authorized users.

Y. Suzuki · H. Hayashi · Y. Nishigaki · E. Tomita
Department of Gastroenterology,
Gifu Municipal Hospital, Gifu, Japan

K. Imai · K. Takai · T. Hanai · T. Naiki · M. Shimizu (✉) · H. Moriwaki
Department of Medicine, Gifu University Graduate School of Medicine, 1-1 Yanagido, Gifu 501-1194, Japan
e-mail: shimim-gif@umin.ac.jp

Published online: 15 February 2013

high α-fetoprotein (AFP), large tumor foci, multiplicity of tumors, pathologically high-grade atypia of tumor cells, and the presence of portal venous invasion of tumors are thought to increase the risk for HCC recurrence (Ikeda et al. 1993; Koike et al. 2000). The increased Homeostatic Model Assessment of Insulin Resistance (HOMA-IR) value, which reflects insulin resistance, and high levels of serum leptin, one of the adipokines associated with obesity, are also independent risk factors for HCC recurrence (Imai et al. 2010; Watanabe et al. 2011).

Increased evidence indicates that continuous oxidative stress, which results from the imbalance between the production of reactive oxygen species (ROS) and the antioxidant defense mechanisms, plays a critical role in the development of various human malignancies, including HCC (Sasaki 2006; Valko et al. 2007; Sakurai et al. 2008). As a major site of metabolism, the liver displays high levels of ROS resulting in increased oxidative stress. Oxidative stress is known to induce DNA damage, and accumulation of such genetic damage can eventually contribute to liver carcinogenesis (Sasaki 2006; Valko et al. 2007; Sakurai et al. 2008). HCV infection is associated with elevated levels of ROS and decreased antioxidant levels in patients (Seronello et al. 2007). Oxidative stress has been associated with the development of steatosis and liver tumors in HCV core transgenic mice (Moriya et al. 2001). In addition, increased levels of ROS is also involved in migration, invasion, and metastasis of HCC cells (Hu et al. 2011; Chung et al. 2012). These findings suggest that oxidative stress biomarkers might potentially be useful for predicting the development and recurrence of HCC in patients with chronic liver disease. Clinical studies using liver specimens obtained by biopsy or surgery have shown the predictive power of oxidative stress biomarkers on HCC development (Chuma et al. 2008; Tanaka et al. 2011). However, serum oxidative stress biomarkers predictive for recurrence after curative treatment for HCC have not been investigated.

Quantification of derivatives of reactive oxygen metabolites (d-ROM) is a simple method for detecting hydroperoxide levels (Trotti et al. 2002), and clinical trials have shown that the d-ROM test is useful for evaluating oxidative stress (Trotti et al. 2002; Hirose et al. 2009; Sugiura et al. 2011). In this study, we measured the serum d-ROM level in patients with HCC and designed a prospective case series analysis to examine the recurrence-free survival in consecutive patients with stage I/II HCC who received curative treatment by surgical resection or radiofrequency ablation (RFA), stratified according to the serum d-ROM level. Thus, the aim of the present study was to determine whether the d-ROM test is useful as a marker of oxidative stress for evaluating HCC recurrence risk in the clinical setting.

## Patients and methods

### Patients

We evaluated 45 consecutive primary HCC patients in Gifu Municipal Hospital from 2006 to 2007, all of whom met the following criteria: tumor stage classified as I or II and surgical resection or RFA as the initial treatment. Tumor stage was defined according to the staging system of the Liver Cancer Study Group of Japan (2010). HCC nodules were detected using imaging modalities including dynamic computed tomography (CT), dynamic magnetic resonance imaging (MRI), and abdominal arteriography. HCC was diagnosed from a typical hypervascular tumor stain on angiography and typical dynamic study findings of enhanced staining in the early phase and attenuation in the delayed phase.

### Treatment, follow-up, and determination of recurrence

One patient was treated with surgical resection, 41 with RFA, and 3 with RFA after transarterial chemoembolization. The selection criteria for the initial treatments were determined according to the Clinical Practice Guidelines for HCC by the Japan Society of Hepatology (Clinical Practice Guidelines for Hepatocellular Carcinoma—The Japan Society of Hepatology 2009 update 2010). The response to treatment was defined as complete response when dynamic CT or MRI showed complete disappearance of the HCC imaging characteristics in all target lesions, according to the Response Evaluation Criteria in Cancer of the Liver (Kudo et al. 2010).

Patients were thereafter followed up on an outpatient basis by assessing the levels of serum tumor markers such as AFP and proteins induced by vitamin K absence or antagonist-II (PIVKA-II) every month and by using imaging modalities such as abdominal ultrasonography, dynamic CT scanning, or dynamic MRI every 3 months. Recurrent HCC was defined as the appearance of distant lesions to exclude local recurrence. Consequently, recurrent HCC was further classified into multicentric occurrence or intrahepatic metastasis by CT images according to the definition by the Liver Cancer Study Group of Japan (Liver Cancer Study Group of Japan 2010). The follow-up period was defined as the interval from the date of initial treatment until the date of diagnosis of recurrence or until March 2012 if HCC did not recur.

### Oxidative stress assay

Before curative treatment, oxidative stress was assessed by measuring the serum hydroperoxide concentration according to the d-ROM test (Diacron srl, Grosseto, Italy) by

**Table 1** Baseline demographic and clinical characteristics

| Variables | $n = 45$ |
|---|---|
| Sex (male/female) | 30/15 |
| Age (years) | 72 [50–82] |
| BMI (kg/m$^2$) | 22.8 [15.6–33.5] |
| Etiology (B/C/B + C/other) | 3/40/1/1 |
| Follow-up period (days) | 1,707 [305–2,231] |
| d-ROM (Carr U) | 496 [295–869] |
| Child-Pugh classification (A/B/C) | 33/12/0 |
| ALB (g/dL) | 3.5 [2.6–4.5] |
| ALT (IU/L) | 51 [12–100] |
| T-Bil (mg/dL) | 1.0 [0.5–3.7] |
| PLT ($\times 10^4/\mu$L) | 9.8 [3.6–19.5] |
| PT (%) | 71 [50–100] |
| FPG (mg/dL) | 100 [41–224] |
| $HbA_{1c}$ (%)[a] | 5.7 [4.0–9.8] |
| AFP (ng/dL) | 32.5 [1.7–16,931] |
| PIVKA-II (mAU/mL) | 23.0 [5–1,860] |
| Stage (I/II) | 21/24 |
| Tumor size (cm) | 1.7 [1.0–5.3] |
| Tumor number (1/2/3/4) | 36/6/1/2 |
| Portal vein invasion (yes/no) | 0/45 |
| Initial treatment for HCC (resection/RFA/TACE + RFA) | 1/41/3 |

Values are presented as median [range]. *BMI* body mass index, *d-ROM* derivatives of reactive oxygen metabolites, *ALB* albumin, *ALT* alanine aminotransferase, *T-Bil* total bilirubin, *PLT* platelet count, *PT* prothrombin time, *FPG* fasting plasma glucose, *$HbA_{1c}$* hemoglobin A1c, *AFP* α-fetoprotein, *PIVKA-II* protein induced by vitamin K absence or antagonists-II, *RFA* radiofrequency ablation, *TACE* transarterial chemoembolization

[a] $HbA_{1c}$ is presented in National Glycohemoglobin Standardization Program units

using a free radical elective evaluator, FREE (Diacron srl), as described previously (Trotti et al. 2002; Hirose et al. 2009; Sugiura et al. 2011).

### Statistical analysis

Recurrence-free survival was estimated using the Kaplan–Meier method, and differences between curves were evaluated using the logrank test. Baseline characteristics were compared using the Student's $t$ test for continuous variables or the $\chi^2$ test for categorical variables. Eleven possible predictors for HCC recurrence after initial curative treatment were selected as follows: sex, age, body mass index (BMI), Child-Pugh classification, serum albumin level, platelet count, fasting plasma glucose (FPG), serum AFP level, serum PIVKA-II level, tumor stage, and the serum d-ROM level. Parameters determined to be significant according to univariate analysis were then subjected to multivariate analysis using the Cox proportional hazards model. Receiver operating characteristic (ROC) analysis was used to identify the cut-off values for d-ROM and AFP that would best predict HCC recurrence. Statistical significance was defined as $P < 0.05$.

## Results

### Baseline characteristics and laboratory data of patients

The baseline characteristics and laboratory data of the 45 patients (30 men and 15 women, median age: 72 years) are shown in Table 1. The median follow-up period was 1,707 days (range 305–2,231 days). Thirty-three patients were classified as Child-Pugh class A, 12 patients as class B, and none as class C. The median d-ROM level of all the patients with HCC was 496 Carr U (range 295–869 Carr U).

### Possible risk factors for HCC recurrence

In all 45 curative cases of stage I/II HCC, 41 patients experienced recurrence in the liver and 2 patients exhibited distant metastasis; 1 in the lung and the other in the bone. The 1-year, 3-year, and 5-year recurrence-free survival rates in the 45 patients were 60, 29, and 7 %, respectively (Fig. 1a). Among 41 cases that caused intrahepatic recurrence of HCC, 36 cases were diagnosed as multicentric occurrence and the others (5 cases) were as intrahepatic metastasis, respectively.

At first, we analyzed possible risk factors for total recurrence including both multicentric occurrence and intrahepatic metastasis by the Cox proportional hazards model using the 11 variables listed in Table 2. The serum d-ROM level (hazard ratio [HR] 1.0036, 95 % confidence interval [CI] 1.0005–1.0070, $P = 0.0231$), serum AFP level (HR 1.0001, 95 % CI 1.0000–1.0002, $P = 0.0274$), and FPG (HR 1.0008, 95 % CI 1.0004–1.0157, $P = 0.0400$) were significantly associated with HCC recurrence in univariate analysis. Among these variables, multivariate analysis indicated that serum levels of d-ROM (HR 1.0038, 95 % CI 1.0002–1.0071, $P = 0.0392$) and AFP (HR 1.0002, 95 % CI 1.0000–1.0003, $P = 0.0316$) were independent predictors of HCC recurrence (Table 3).

The cut-off values of d-ROM (570 Carr U) and AFP (40 ng/dL) for the prediction of HCC recurrence were determined by ROC analysis. Kaplan–Meier analysis showed that recurrence-free survival was lower in patients with high serum d-ROM levels (≥570 Carr U, $P = 0.0036$) (Fig. 1b) and in those with high serum AFP levels (≥40 ng/dL, $P = 0.0185$) (Fig. 1c). Table 4 shows the baseline characteristics and laboratory data of patients

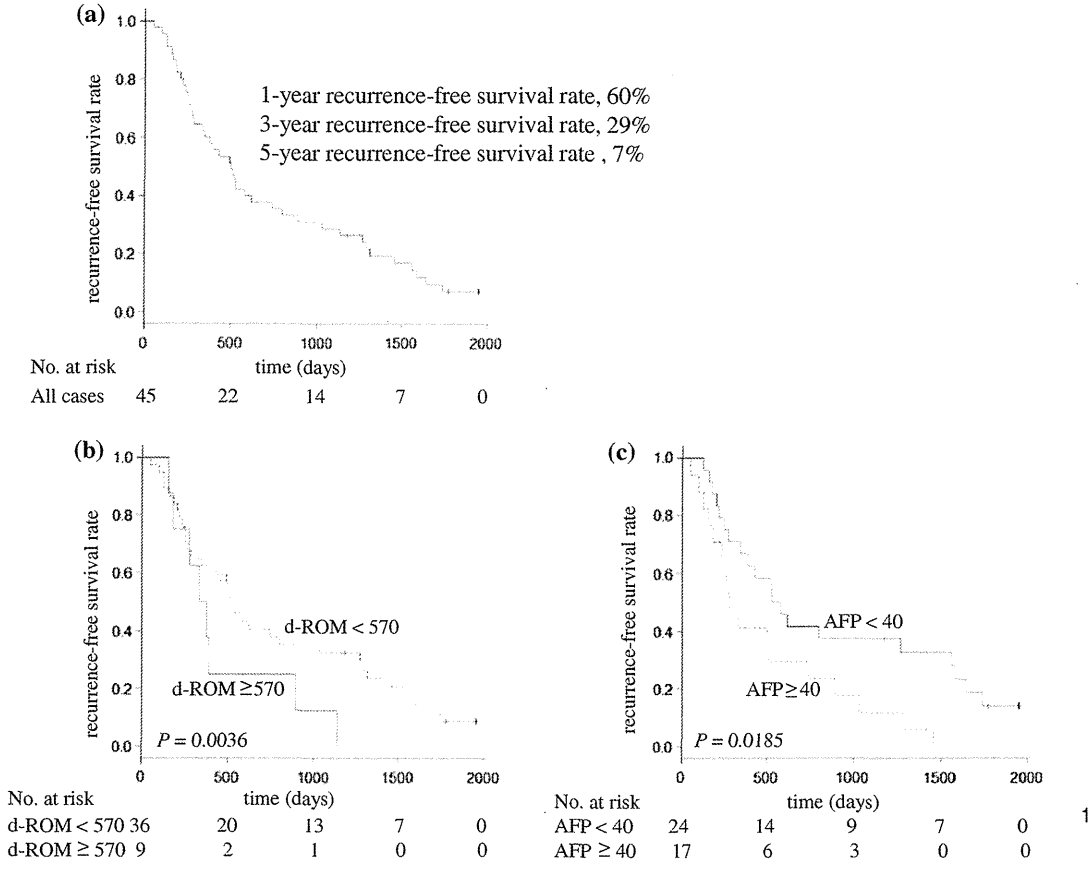


**Fig. 1** Kaplan–Meier curves for recurrence-free survival in (**a**) all patients and in subgroups of patients, divided according to (**b**) d-ROM levels or (**c**) serum AFP levels

**Table 2** Univariate analyses of possible risk factors for hepatocellular carcinoma recurrence according to a Cox proportional hazards model

| Variable | HR | 95 % CI | | *P* value |
|---|---|---|---|---|
| | | Lower limit | Upper limit | |
| Sex (male vs. female) | 0.9142 | 0.4810 | 1.8307 | 0.7917 |
| Age (years) | 1.0086 | 0.9714 | 1.0473 | 0.6522 |
| BMI (kg/m$^2$) | 0.9878 | 0.9082 | 1.0696 | 0.7695 |
| Child-Pugh classification (B vs. A) | 0.9707 | 0.4643 | 1.8843 | 0.9329 |
| ALB (g/dL) | 0.9496 | 0.4600 | 1.9744 | 0.8893 |
| PLT ($\times 10^4$/mL) | 0.9817 | 0.9031 | 1.0613 | 0.6507 |
| FPG (mg/dL) | 1.0008 | 1.0004 | 1.0157 | 0.0400 |
| AFP (ng/dL) | 1.0001 | 1.0000 | 1.0002 | 0.0274 |
| PIVKA-II (mAU/mL) | 1.0005 | 0.9996 | 1.0012 | 0.2149 |
| Stage (II vs. I) | 1.1968 | 0.6468 | 2.2348 | 0.5664 |
| d-ROM (Carr U) | 1.0036 | 1.0005 | 1.0070 | 0.0231 |

*CI* confidence interval, *HR* hazard radio, *BMI* body mass index, *ALB* albumin, *PLT* platelets, *FPG* fasting plasma glucose, *AFP* α-fetoprotein, *PIVKA-II* protein induced by vitamin K absence or antagonists-II, *d-ROM* derivatives of reactive oxygen metabolites

divided on the basis of the serum d-ROM concentration (<570 Carr U and ≥ 570 Carr U). No significant differences were noted between the 2 subgroups.

The serum d-ROM levels were not significantly correlated with any clinical factors associated with hepatic functional reserve (serum total bilirubin, serum albumin,

**Table 3** Multivariate analyses of possible risk factors for hepatocellular carcinoma recurrence according to a Cox proportional hazards model

| Variable | HR | 95 % CI | | *P* value |
|---|---|---|---|---|
| | | Lower limit | Upper limit | |
| FPG (mg/dL) | 1.0004 | 0.9961 | 1.0126 | 0.2699 |
| AFP (ng/dL) | 1.0002 | 1.0000 | 1.0003 | 0.0316 |
| d-ROM (Carr U) | 1.0038 | 1.0002 | 1.0071 | 0.0392 |

*CI* confidence interval, *HR* hazard radio, *FPG* fasting plasma glucose, *AFP* α-fetoprotein, *d-ROM* derivatives of reactive oxygen metabolites

serum alanine aminotransferase, prothrombin time, and platelet count) and HCC (tumor size, AFP, and PIVKA-II) (Table 5). In addition, the d-ROM levels did not show significant relationships between the clinical factors for diabetes, including FPG, $HbA_{1c}$, fasting immunoreactive insulin, and HOMA-IR (Table 5), although several studies have reported that oxidative stress increases with the presence of diabetes and that the d-ROM level is correlated with diabetic factors (Vassalle et al. 2008; Hirose et al. 2009; Sugiura et al. 2011). Further, no significant differences in the median values of d-ROM were noted between (1) the Child-Pugh class A group (496 Carr U, range 295–869 Carr U) and the Child-Pugh class B group (500 Carr U, range 314–589 Carr U) and (2) the stage I group (516 Carr U, range 295–858 Carr U) and the stage II group (500 Carr U, range 314–869 Carr U), suggesting that d-ROM values were not associated with hepatic functional reserve, tumor factors, or the presence of diabetes in this study. These findings indicate that an increased d-ROM value was independently related to the recurrence of HCC.

A separate analysis of 36 multicentric occurrence cases showed an inverse correlation between the serum d-ROM levels and the recurrence-free period, but the significance was marginal ($P = 0.0512$) due to the small number of patients (data not shown). In addition, intrahepatic metastasis cases ($N = 5$) showed a higher d-ROM levels (median 614 Carr U, range 496–869 Carr U) than non-recurrent cases ($N = 4$, median 474 Carr U, range: 461–509 Carr U) ($P = 0.112$).

## Discussion

Increasing evidence suggests that oxidative stress plays a critical role in liver carcinogenesis (Sasaki 2006; Sakurai et al. 2008). Elevation of ROS can cause oxidative damage to important cellular macromolecules such as DNA, proteins, and lipids (Valko et al. 2007). Excessive ROS also disrupts the cell signaling pathways that are involved in cell growth and survival, leading further to the advanced stage of carcinogenesis, and cancer promotion and progression (Dreher and Junod 1996; Carmeliet 2000).

**Table 4** Baseline demographic and clinical characteristics of patients classified according to the d-ROM level

| | d-ROMs < 570 ($n = 36$) | d-ROMs ≥ 570 ($n = 9$) | *P* value |
|---|---|---|---|
| Sex (male/female) | 24/12 | 6/3 | 1.0000 |
| Age (years) | 72 [50–82] | 69 [58–76] | 0.5325 |
| BMI | 22.5 [15.6–33.5] | 23.0 [20.1–27.0] | 0.7965 |
| Etiology (B/C/B + C/other) | 3/31/1/1 | 0/9/0/0 | 0.4968 |
| Follow-up period (days) | 1,712 [458–2,231] | 1,643 [305–2,146] | 0.2350 |
| Child-Pugh classification (A/B) | 26/10 | 7/2 | 0.7323 |
| ALB (g/dL) | 3.5 [2.6–4.5] | 3.5 [3.0–4.4] | 0.9312 |
| ALT (IU/L) | 48 [12–100] | 53 [22–73] | 0.5621 |
| T-Bil (mg/dL) | 1.0 [0.5–3.7] | 1.0 [0.6–1.5] | 0.8532 |
| PLT ($\times 10^4/\mu L$) | 10.4 [3.8–19.5] | 6.6 [3.6–18.8] | 0.0843 |
| PT (%) | 70 [50–100] | 77 [59–90] | 0.2293 |
| FPG (mg/dL) | 99 [41–224] | 104 [83–140] | 0.6272 |
| $HbA_{1c}$ (%)[a] | 5.7 [4.0–9.8] | 5.3 [4.8–7.0] | 0.6447 |
| AFP (ng/dL) | 31 [1.7–16,931] | 33 [16.7–210] | 0.5130 |
| PIVKA-II (mAU/mL) | 19.5 [5–1,540] | 57.0 [7–1,860] | 0.2822 |
| Stage (I/II) | 17/19 | 4/5 | 0.8811 |
| Initial treatment for HCC (resection/RFA/TACE + RFA) | 1/32/3 | 0/9/0 | 0.3905 |

Values are presented as median [range]. *BMI* body mass index, *ALB* albumin, *ALT* alanine aminotransferase, *T-Bil* total bilirubin, *PLT* platelets, *PT* prothrombin time, *FPG* fasting plasma glucose, *$HbA_{1c}$* hemoglobin A1c, *AFP* α-fetoprotein, *PIVKA-II* protein induced by vitamin K absence or antagonists-II, *HCC* hepatocellular carcinoma

[a] $HbA_{1c}$ is presented in National Glycohemoglobin Standardization Program units

**Table 5** Correlation between clinical factors and d-ROM using linear regression analysis

| | Pearson's correlation coefficient | *P* value |
|---|---|---|
| ALB (g/dL) | −0.0073 | 0.9621 |
| ALT (IU/L) | −0.1007 | 0.5153 |
| T-Bil (mg/dL) | −0.0044 | 0.9771 |
| PLT ($\times 10^4/\mu L$) | −0.2319 | 0.1254 |
| PT (%) | 0.2045 | 0.1777 |
| FPG (mg/dL) | 0.0013 | 0.9935 |
| $HbA_{1c}$ (%) | −0.1225 | 0.5043 |
| FIRI (mg/dL) | −0.0740 | 0.6924 |
| HOMA-IR | −0.1590 | 0.3271 |
| AFP (ng/dL) | −0.1696 | 0.2892 |
| PIVKA-II (mAU/mL) | −0.0263 | 0.8798 |
| Tumor size (cm) | −0.1969 | 0.2074 |

*ALB* albumin, *ALT* alanine aminotransferase, *T-Bil* total bilirubin, *PLT* platelets, *PT* prothrombin time, *FPG* fasting plasma glucose, *$HbA_{1c}$* hemoglobin A1c, *FIRI* fasting immunoreactive insulin, *HOMA-IR* Homeostatic Model Assessment of Insulin Resistance, *AFP* α-fetoprotein, *PIVKA-II* protein induced by vitamin K absence or antagonists-II

[a] $HbA_{1c}$ is presented in National Glycohemoglobin Standardization Program units

In the present study, HCC recurrence was noted in patients with high serum d-ROM levels (≥570 Carr U, $P = 0.0036$, Fig. 1b) that reflect increased oxidative stress (Trotti et al. 2002). In particular, the 2-year recurrence rate was higher in patients with high serum d-ROM levels (Fig. 1b). We presume that this is primarily associated with the clinical characteristic mode of liver carcinogenesis, that is multicentric carcinogenesis, (occurrence) because when the whole liver was exposed to increased oxidative stress for a long duration, multiple malignant clones that can progress to HCC in the future may have been produced. In our multicentric occurrence cases ($N = 36$), an inverse correlation was actually found between d-ROM levels and recurrence-free period. In addition, intrahepatic metastasis cases showed higher d-ROM levels than non-recurrent patients. These results of the present study, together with recent reports showing the promoting effects of oxidative stress on migration, invasion, and metastasis of HCC cells (Hu et al. 2011; Chung et al. 2012), indicate that intrahepatic metastasis might also be involved, together with multicentric occurrence, in the increase in the 2-year recurrence rate. This finding suggests that increased oxidative stress is a risk factor for HCC development and that the d-ROM test could be a useful clinical diagnostic tool to predict the recurrence of HCC.

A recent clinical trial revealed that loss of the expression of CYP1A2, a major component of the hepatic cytochrome P450 oxidative system, in non-cancerous tissue is a predictive factor of recurrence after curative hepatectomy for early-stage HCC (Tanaka et al. 2011). High levels of 8-hydroxy-2′-deoxyguanosine (8-OHdG), a marker of DNA damage caused by ROS, in liver biopsy specimens is also a risk factor for HCC development in patients with chronic HCV infection (Chuma et al. 2008). These reports (Chuma et al. 2008; Tanaka et al. 2011), together with the results of the present study, strongly suggest that oxidative stress biomarkers are useful for evaluating patients at a high risk for HCC development. In particular, the results of this study are clinically relevant because the d-ROM test can be performed easily by using serum, whereas the methods used in previous studies involve the use of liver tissues obtained by invasive surgery or biopsy (Chuma et al. 2008; Tanaka et al. 2011).

Increased production of free radicals at the site of inflammation and subsequent oxidative DNA damage is a strong mechanistic link between chronic inflammation and carcinogenesis (Hussain et al. 2003). Oxidative stress is involved in chronic liver inflammation induced by viral hepatitis, alcoholic hepatitis, and non-alcoholic steatohepatitis (Day and James 1998; Loguercio and Federico 2003; Siegel and Zhu 2009). Oxidative DNA damage is enhanced in serum and liver specimens of patients with HCV infection (Sumida et al. 2000; Mahmood et al. 2004). A strong positive correlation between inflammation, intrahepatic oxidative stress, and oxidative DNA damage are also observed in the liver of HCV-associated HCC patients (Maki et al. 2007). In the present study, the median d-ROM level of all the patients with HCC was 496 Carr U (Table 1), and this value is much higher than that of healthy control individuals (250–300 Carr U) (Trotti et al. 2002). This finding may suggest that the systemic level of oxidative stress caused by liver inflammation is increased in HCC patients. The usefulness of the d-ROM test for evaluating the correlation between increased levels of systemic inflammation and oxidative stress has also been reported in previous clinical studies (Trotti et al. 2002; Hirose et al. 2009; Sugiura et al. 2011).

The present study included 3 HCV-positive patients who received interferon therapy to eliminate the virus before HCC development. Two of these patients demonstrated a sustained virological response (SVR); however, all of them showed recurrence of HCC. Three additional HCV-positive patients also received interferon therapy to prevent HCC recurrence after the initial HCC development, but none of them showed a SVR, and 2 patients suffered a relapse. The serum d-ROM levels of the enrolled patients during the follow-up period, including after curative treatment as well as at the recurrence points, were not examined in the present study. However, these measurements seem to be significant and should be performed in future studies because the levels of d-ROM might be useful as a

biomarker for assessing the effectiveness of treatment for chronic liver diseases with interferon (Morisco et al. 2004). The d-ROM test was used in a clinical trial to evaluate oxidative status as a predictive factor of the therapeutic response of interferon and ribavirin treatment in patients with chronic hepatitis C (Morisco et al. 2004). In the study, the patients with a successive long-term response had lower d-ROM levels than non-responders (Morisco et al. 2004), suggesting that the serum levels of d-ROM might help to predict long-term response to interferon/ribavirin therapy in patients with chronic viral hepatitis. Moreover, this report also suggested that antiviral therapy could possibly attenuate oxidative stress because the mean d-ROM levels were significantly decreased during the treatment (Morisco et al. 2004). Iron depletion, which can decrease the production of ROS, improves the end-of-treatment biological and histological response to interferon therapy (Fontana et al. 2000). Iron reduction also decreases the levels of 8-OHdG and risk of HCC in HCV patients (Kato et al. 2001). Future studies to determine whether targeting oxidative stress is useful for the treatment of chronic liver disease, including the prevention of HCC, and whether the d-ROM test is applicable for evaluating oxidative stress should be conducted.

Finally, in addition to the production of ROS, alteration in the antioxidant activity is also implicated in imbalance of the normal redox state and subsequent liver carcinogenesis (Sasaki 2006; Valko et al. 2007; Sakurai et al. 2008). Experimental studies have shown evidence that dietary antioxidants, for example, vitamin E, vitamin C, and selenium, play a possible role in the prevention of liver carcinogenesis (Glauert et al. 2010). Therefore, intervention trials to examine whether antioxidant supplementation decreases the serum d-ROM levels and, therefore, possibly inhibits the development of HCC should be conducted in the future. On the other hand, several clinical studies have shown that antioxidant activity is induced as an adaptive response to increased generation of ROS in patients with HCC (Clemente et al. 2007; Abel et al. 2009; Tsai et al. 2009). An increase in the activity of manganese superoxide dismutase, an antioxidant enzyme, occurs during the precancerous phase and serves as a potential biomarker for HCC (Clemente et al. 2007). Disruption of the redox balance, resulting in increased cellular antioxidant capacity, might also create an advantageous environment for the growth of HBV-associated HCC cells (Abel et al. 2009). These reports suggest that antioxidant activity could be a predictive factor for the development of HCC.

In conclusion, this is the first indication that stage I/II patients curatively treated using surgical resection or RFA who have increased serum d-ROM levels, which reflect increased oxidative stress, are liable to HCC recurrence. The d-ROM test can be used for screening patients at a high risk for HCC recurrence, and those who show increased d-ROM levels may require careful surveillance.

**Acknowledgments** This work was supported in part by Grants-in-Aid from the Ministry of Education, Science, Sports and Culture of Japan (No. 22790638 to M. S. and No. 21590838 to H. M.) and by Grant-in-Aid for the 3rd Term Comprehensive 10-Year Strategy for Cancer Control from the Ministry of Health, Labour and Welfare of Japan.

**Conflict of interest** The authors declare no conflict of interest.

## References

Abel S, De Kock M, van Schalkwyk DJ, Swanevelder S, Kew MC, Gelderblom WC (2009) Altered lipid profile, oxidative status and hepatitis B virus interactions in human hepatocellular carcinoma. Prostaglandins Leukot Essent Fat Acids 81(5–6): 391–399. doi:10.1016/j.plefa.2009.08.003

Carmeliet P (2000) Mechanisms of angiogenesis and arteriogenesis. Nat Med 6(4):389–395. doi:10.1038/74651

Chuma M, Hige S, Nakanishi M, Ogawa K, Natsuizaka M, Yamamoto Y, Asaka M (2008) 8-Hydroxy-2′-deoxy-guanosine is a risk factor for development of hepatocellular carcinoma in patients with chronic hepatitis C virus infection. J Gastroenterol Hepatol 23(9):1431–1436. doi:10.1111/j.1440-1746.2008.05502.x

Chung JS, Park S, Park SH, Park ER, Cha PH, Kim BY, Chung YM, Woo SR, Han CJ, Kim SB, Suh KS, Jang JJ, Lee K, Choi DW, Lee S, Lee GY, Hahm KB, Shin JA, Kim BS, Noh KH, Kim TW, Lee KH, Yoo YD (2012) Overexpression of Romo1 promotes production of reactive oxygen species and invasiveness of hepatic tumor cells. Gastroenterology 143(4):1084–1094 e1087. doi:10.1053/j.gastro.2012.06.038

Clemente C, Elba S, Buongiorno G, Guerra V, D'Attoma B, Orlando A, Russo F (2007) Manganese superoxide dismutase activity and incidence of hepatocellular carcinoma in patients with Child-Pugh class A liver cirrhosis: a 7-year follow-up study. Liver Int Off J Int Assoc Study Liver 27(6):791–797. doi:10.1111/j.1478-3231.2007.01485.x

Clinical Practice Guidelines for Hepatocellular Carcinoma (2010) The Japan Society of Hepatology 2009 update. Hepatol Res Off J Jpn Soc Hepatol 40(Suppl 1):2–144. doi:10.1111/j.1872-034X.2010.00650.x

Day CP, James OF (1998) Steatohepatitis: a tale of two "hits"? Gastroenterology 114(4):842–845

Dreher D, Junod AF (1996) Role of oxygen free radicals in cancer development. Eur J Cancer 32A(1):30–38

El-Serag HB (2002) Hepatocellular carcinoma: an epidemiologic view. J Clin Gastroenterol 35(5 Suppl 2):S72–S78

Fontana RJ, Israel J, LeClair P, Banner BF, Tortorelli K, Grace N, Levine RA, Fiarman G, Thiim M, Tavill AS, Bonkovsky HL (2000) Iron reduction before and during interferon therapy of chronic hepatitis C: results of a multicenter, randomized, controlled trial. Hepatology 31(3):730–736. doi:10.1002/hep.510310325

Glauert HP, Calfee-Mason K, Stemm DN, Tharappel JC, Spear BT (2010) Dietary antioxidants in the prevention of hepatocarcinogenesis: a review. Mol Nutr Food Res 54(7):875–896. doi:10.1002/mnfr.200900482

Hirose H, Kawabe H, Komiya N, Saito I (2009) Relations between serum reactive oxygen metabolites (ROMs) and various inflammatory and metabolic parameters in a Japanese population. J Atheroscler Thromb 16(2):77–82

Hu CT, Wu JR, Cheng CC, Wang S, Wang HT, Lee MC, Wang LJ, Pan SM, Chang TY, Wu WS (2011) Reactive oxygen species-mediated PKC and integrin signaling promotes tumor progression of human hepatoma HepG2. Clin Exp Metastasis 28(8):851–863. doi:10.1007/s10585-011-9416-6

Hussain SP, Hofseth LJ, Harris CC (2003) Radical causes of cancer. Nat Rev Cancer 3(4):276–285. doi:10.1038/nrc1046

Ikeda K, Saitoh S, Tsubota A, Arase Y, Chayama K, Kumada H, Watanabe G, Tsurumaru M (1993) Risk factors for tumor recurrence and prognosis after curative resection of hepatocellular carcinoma. Cancer 71(1):19–25

Imai K, Takai K, Nishigaki Y, Shimizu S, Naiki T, Hayashi H, Uematsu T, Sugihara J, Tomita E, Shimizu M, Nagaki M, Moriwaki H (2010) Insulin resistance raises the risk for recurrence of stage I hepatocellular carcinoma after curative radiofrequency ablation in hepatitis C virus-positive patients: a prospective, case series study. Hepatol Res Off J Jpn Soc Hepatol 40(4):376–382. doi:10.1111/j.1872-034X.2009.00616.x

Jemal A, Bray F, Center MM, Ferlay J, Ward E, Forman D (2011) Global cancer statistics. CA Cancer J Clin 61(2):69–90. doi:10.3322/caac.20107

Kato J, Kobune M, Nakamura T, Kuroiwa G, Takada K, Takimoto R, Sato Y, Fujikawa K, Takahashi M, Takayama T, Ikeda T, Niitsu Y (2001) Normalization of elevated hepatic 8-hydroxy-2′-deoxyguanosine levels in chronic hepatitis C patients by phlebotomy and low iron diet. Cancer Res 61(24):8697–8702

Koike Y, Shiratori Y, Sato S, Obi S, Teratani T, Imamura M, Hamamura K, Imai Y, Yoshida H, Shiina S, Omata M (2000) Risk factors for recurring hepatocellular carcinoma differ according to infected hepatitis virus-an analysis of 236 consecutive patients with a single lesion. Hepatology 32(6):1216–1223. doi:10.1053/jhep.2000.20237

Kudo M, Kubo S, Takayasu K, Sakamoto M, Tanaka M, Ikai I, Furuse J, Nakamura K, Makuuchi M (2010) Response evaluation criteria in cancer of the liver (RECICL) proposed by the Liver Cancer Study Group of Japan (2009 revised version). Hepatol Res Off J Jpn Soc Hepatol 40(7):686–692. doi:10.1111/j.1872-034X.2010.00674.x

Liver Cancer Study Group of Japan (2010) General rules for the clinical and pathological study of primary liver cancer, 3rd English edn. Kanehara & Co., Ltd., Tokyo

Loguercio C, Federico A (2003) Oxidative stress in viral and alcoholic hepatitis. Free Radic Biol Med 34(1):1–10

Mahmood S, Kawanaka M, Kamei A, Izumi A, Nakata K, Niiyama G, Ikeda H, Hanano S, Suehiro M, Togawa K, Yamada G (2004) Immunohistochemical evaluation of oxidative stress markers in chronic hepatitis C. Antioxid Redox Signal 6(1):19–24. doi:10.1089/152308604771978318

Maki A, Kono H, Gupta M, Asakawa M, Suzuki T, Matsuda M, Fujii H, Rusyn I (2007) Predictive power of biomarkers of oxidative stress and inflammation in patients with hepatitis C virus-associated hepatocellular carcinoma. Ann Surg Oncol 14(3):1182–1190. doi:10.1245/s10434-006-9049-1

Morisco F, Verde V, Fogliano V, Ritieni A, Marmo R, De Luise G, Tuccillo C, Caporaso N (2004) Oxidative status in chronic hepatitis C: the influence of antiviral therapy and prognostic value of serum hydroperoxide assay. Free Radic Res 38(6):573–580

Moriya K, Nakagawa K, Santa T, Shintani Y, Fujie H, Miyoshi H, Tsutsumi T, Miyazawa T, Ishibashi K, Horie T, Imai K, Todoroki T, Kimura S, Koike K (2001) Oxidative stress in the absence of inflammation in a mouse model for hepatitis C virus-associated hepatocarcinogenesis. Cancer Res 61(11):4365–4370

Sakurai T, He G, Matsuzawa A, Yu GY, Maeda S, Hardiman G, Karin M (2008) Hepatocyte necrosis induced by oxidative stress and IL-1 alpha release mediate carcinogen-induced compensatory proliferation and liver tumorigenesis. Cancer Cell 14(2):156–165. doi:10.1016/j.ccr.2008.06.016

Sasaki Y (2006) Does oxidative stress participate in the development of hepatocellular carcinoma? J Gastroenterol 41(12):1135–1148. doi:10.1007/s00535-006-1982-z

Seronello S, Sheikh MY, Choi J (2007) Redox regulation of hepatitis C in nonalcoholic and alcoholic liver. Free Radic Biol Med 43(6):869–882. doi:10.1016/j.freeradbiomed.2007.05.036

Siegel AB, Zhu AX (2009) Metabolic syndrome and hepatocellular carcinoma: two growing epidemics with a potential link. Cancer 115(24):5651–5661. doi:10.1002/cncr.24687

Sugiura T, Dohi Y, Takase H, Yamashita S, Tanaka S, Kimura G (2011) Increased reactive oxygen metabolites is associated with cardiovascular risk factors and vascular endothelial damage in middle-aged Japanese subjects. Vasc Health Risk Manag 7:475–482. doi:10.2147/VHRM.S23097

Sumida Y, Nakashima T, Yoh T, Nakajima Y, Ishikawa H, Mitsuyoshi H, Sakamoto Y, Okanoue T, Kashima K, Nakamura H, Yodoi J (2000) Serum thioredoxin levels as an indicator of oxidative stress in patients with hepatitis C virus infection. J Hepatol 33(4):616–622

Tanaka S, Mogushi K, Yasen M, Ban D, Noguchi N, Irie T, Kudo A, Nakamura N, Tanaka H, Yamamoto M, Kokudo N, Takayama T, Kawasaki S, Sakamoto M, Arii S (2011) Oxidative stress pathways in noncancerous human liver tissue to predict hepatocellular carcinoma recurrence: a prospective, multicenter study. Hepatology 54(4):1273–1281. doi:10.1002/hep.24536

Toyama T, Hiramatsu N, Yakushijin T, Oze T, Nakanishi F, Yasumaru M, Mochizuki K, Kanto T, Takehara T, Kasahara A, Hayashi N (2008) A new prognostic system for hepatocellular carcinoma including recurrent cases: a study of 861 patients in a single institution. J Clin Gastroenterol 42(3):317–322. doi:10.1097/MCG.0b013e3180ebe790

Trotti R, Carratelli M, Barbieri M (2002) Performance and clinical application of a new, fast method for the detection of hydroperoxides in serum. Panminerva Med 44(1):37–40

Tsai SM, Lin SK, Lee KT, Hsiao JK, Huang JC, Wu SH, Ma H, Wu SH, Tsai LY (2009) Evaluation of redox statuses in patients with hepatitis B virus-associated hepatocellular carcinoma. Ann Clin Biochem 46(Pt 5):394–400. doi:10.1258/acb.2009.009029

Valko M, Leibfritz D, Moncol J, Cronin MT, Mazur M, Telser J (2007) Free radicals and antioxidants in normal physiological functions and human disease. Int J Biochem Cell Biol 39(1):44–84. doi:10.1016/j.biocel.2006.07.001

Vassalle C, Pratali L, Boni C, Mercuri A, Ndreu R (2008) An oxidative stress score as a combined measure of the pro-oxidant and anti-oxidant counterparts in patients with coronary artery disease. Clin Biochem 41(14–15):1162–1167. doi:10.1016/j.clinbiochem.2008.07.005

Watanabe N, Takai K, Imai K, Shimizu M, Naiki T, Nagaki M, Moriwaki H (2011) Increased levels of serum leptin are a risk factor for the recurrence of stage I/II hepatocellular carcinoma after curative treatment. J Clin Biochem Nutr 49(3):153–158. doi:10.3164/jcbn.10-149

Semin Immunopathol (2013) 35:191–202
DOI 10.1007/s00281-012-0336-6

REVIEW

# Obesity and hepatocellular carcinoma: targeting obesity-related inflammation for chemoprevention of liver carcinogenesis

**Masahito Shimizu · Takuji Tanaka · Hisataka Moriwaki**

Received: 25 June 2012 / Accepted: 16 August 2012 / Published online: 4 September 2012


**Abstract** Obesity and related metabolic abnormalities, including a state of chronic inflammation, increase the risk of hepatocellular carcinoma (HCC). Adipose tissue constitutively expresses the proinflammatory cytokine tumor necrosis factor-α (TNF-α) and interleukin-6 (IL-6), which are important tumor promoters in inflammation-related carcinogenesis. Dysregulation of TNF-α and IL-6 is associated with the development of steatosis and inflammation within the liver. These cytokines also lie at the core of the association between obesity and insulin resistance, which is a key factor in the development of obesity-related HCC. Here we present a detailed review of the relationship between metabolic abnormalities and the development of HCC, focusing on the role played by inflammation. Drawing from our basic and clinical research, the present report also reviews evidence that targeting metabolic abnormalities, such as attenuation of chronic inflammation and improvement of insulin resistance by either pharmaceutical or nutritional intervention, may be an effective strategy in preventing the development of HCC in obese individuals.

**Keywords** Obesity · Inflammation · Hepatocellular carcinoma · Chemoprevention

This article is a contribution to the special issue on Inflammation and Cancer - Guest Editor: Takuji Tanaka

This article is published as part of the Special Issue on *Inflammation and Cancer* [35:2].

M. Shimizu (✉) · H. Moriwaki
Department of Gastroenterology, Gifu University Graduate School of Medicine,
1-1 Yanagido,
Gifu 501-1194, Japan
e-mail: shimim-gif@umin.ac.jp

T. Tanaka
The Tohkai Cytopathology Institute: Cancer Research and Prevention (TCI-CaRP),
Gifu 500-8285, Japan

## Introduction

Obesity, a condition resulting from an excess of adipose tissue, is currently a serious health problem throughout the world, with approximately 1.6 billion overweight and 500 million obese adults [1]. Numerous health disorders complicate obesity, including cardiovascular disease, hypertension, insulin resistance, diabetes mellitus, and hyperlipidemia, which are collectively known as "metabolic syndrome." Non-alcoholic fatty liver disease (NAFLD), which is known to be a hepatic manifestation of metabolic syndrome, is also the most common form of chronic liver disease in developed countries [2, 3]. In addition, recently, obesity and its related metabolic abnormalities, especially diabetes mellitus, have been recognized as major risk factors for the development of certain types of human malignancies, including hepatocellular carcinoma (HCC) [4–16]. A prospective study of a population of more than 900,000 American adults showed that a higher body mass index (BMI) is significantly associated with higher rates of death from cancer, including HCC [17].

Mounting evidence obtained from experimental and epidemiological studies indicates that several pathophysiological mechanisms link obesity and liver carcinogenesis, including the emergence of insulin resistance, alterations in the insulin-like growth factor-1 (IGF-1)/IGF-1 receptor (IGF-1R) axis, a state of chronic inflammation, induction of oxidative stress, and the occurrence of adipokine imbalance [4–8]. Insulin resistance leads to an increased expression of proinflammatory cytokine tumor necrosis factor-α (TNF-α) and interleukin-6 (IL-6), central mediators of chronic inflammatory diseases, and their dysregulation is associated with the development of steatosis and inflammation within the liver [4–8]. Therefore, among obesity-related pathophysiological conditions that cooperatively enhance the development of HCC, insulin resistance and the subsequent inflammatory cascade are thought to play a critical role in the development of HCC [4–8]. On the other hand, studies